ACS OMEGA

Open Access



http://pubs.acs.org/journal/acsodf

Review

# Recent Advances on the Gas-Sensing Properties and Mechanism of Perovskite Oxide Materials - A Review

Nafis Ahmad, Prakash Kanjariya, G. Padma Priya, Anjan Kumar, Rishabh Thakur, RSK Sharma, Mukesh Kumari, Sharnjeet Kaur, and Manoj Kumar Mishra*

Cite This: *ACS Omega* 2025, 10, 13780−13796

Read Online

ACCESS | Metrics & More | Article Recommendations

**ABSTRACT:** Perovskite oxide-based materials ($ABO_3$) have gained much attention as promising candidates for advanced gas-sensing applications due to their versatile structures, tunable properties, and excellent stability. This review discusses recent developments in the synthesis, structural optimization, and functionalization of perovskites to enhance their gas-sensing performance. Strategies such as doping, creating oxygen vacancies, tuning morphology, and forming heterojunctions have significantly improved their sensitivity, selectivity, response, and recovery times. Specific advances include the incorporation of nanostructures, porous morphologies, and catalytic elements, which have optimized the adsorption and desorption processes for various target gases, including volatile organic compounds, $NO_2$, and $CO_2$. Mechanistic insights into the role of oxygen vacancies, surface defects, and charge carrier dynamics are also addressed. These developments position perovskite materials as important components in next-generation gas sensors for environmental monitoring and industrial applications.

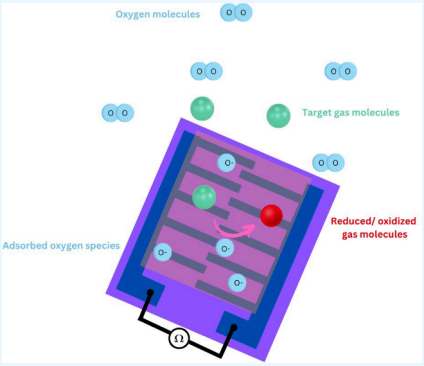


## 1. INTRODUCTION

In recent decades, rapid urban and industrial expansion has led to severe air pollution. Poor air quality poses considerable dangers to human health, especially from the leakage of flammable and toxic gases. As a result, gas sensing technologies have become crucial for monitoring air quality, detecting hazardous gases, and identifying volatile organic compounds (VOCs), as well as in medical diagnostics. Recently, numerous gas sensors have been developed and categorized based on their sensing mechanisms, including thermal conductivity, semiconductor metal oxides (SMOs), infrared absorption, catalytic combustion, electrochemical, and solid electrolyte sensors. Among these, SMO-based gas sensors have emerged as highly promising candidates due to their cost-effectiveness, high sensitivity, ease of use, miniaturization, and flexible fabrication processes.[1,2] Various SMO nanocomposites, such as tin oxide ($SnO_2$),[3] zinc oxide (ZnO),[4] and ferric oxide ($Fe_2O_3$),[5] have been explored for detecting different gases across various applications. Despite this progress, still some challenges exist in developing gas sensors that offer excellent selectivity, high sensitivity, fast response and recovery times, low detection limits, reliable repeatability, long-term stability, and strong resistance to humidity.[6]

In recent years, research has increasingly focused on the development of innovative low-dimensional nanomaterials to boost the gas sensors' performance. Materials such as graphene,[7] carbon nanotubes,[8] metal oxides,[3] and perovskites[9] have emerged as promising candidates due to their excellent electrical properties, mechanical strength, and high surface-to-volume ratios. These materials have demonstrated high sensitivity to gases like $NO_2$, $NH_3$, $H_2S$, $H_2$, and $CO_2$, making them valuable for advanced sensing applications.[10]

The perovskite structure was first discovered by Gustav Rose in 1839 in Russia, within the naturally occurring mineral $CaTiO_3$. Since then, other minerals and synthetic compounds with the general formula $ABX_3$ have been found to share a structure similar to that of $CaTiO_3$, and these are broadly referred to as perovskites. In this structure, the "A" site typically consists of an alkali metal ($A^+$), an alkaline earth metal ($A^{2+}$), or a transition-metal cation ($A^{3+}$) with 12-fold coordination. The "B" site is occupied by transition-metal cations ($B^{3+}$, $B^{4+}$, or $B^{5+}$) with a 6-fold coordination, while "X" represents anions such as oxygen, carbon, nitrogen, or halogens.[11] This kind of material shows good thermal stability and band gap of 3−4 eV and was utilized in several gas sensing studies.[12] Partially or fully replacing A or B cations in the perovskite structure with lower valence cations, reducing their total charge to less than 6+,

Received: December 29, 2024
Revised: February 25, 2025
Accepted: March 26, 2025
Published: April 1, 2025

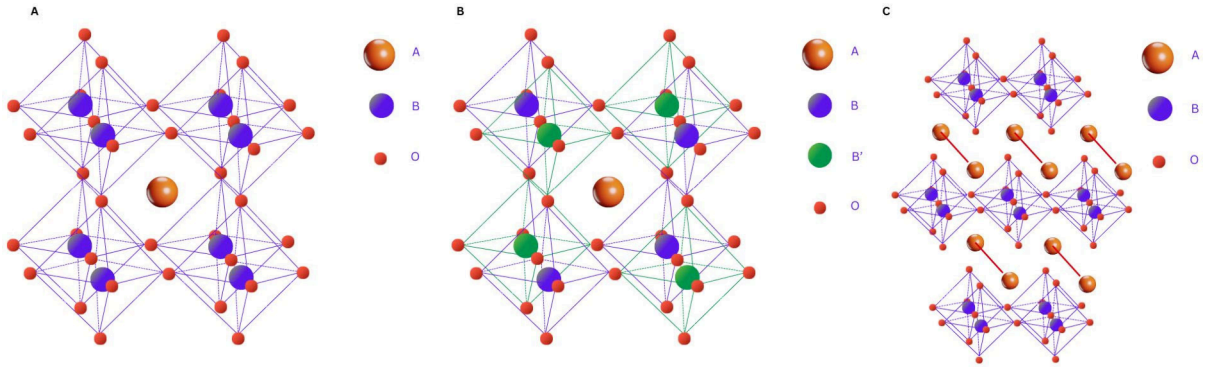


**Figure 1.** Schematic illustration of the A) simple perovskite structure, B) double perovskite, and C) layered perovskite.

creates vacancies in the oxygen lattice. This modification enables mixed ionic and electronic conductivities, where the transition-metal cations contribute to electronic conductivity. Nanomaterial-based perovskite materials have shown excellent sensing ability toward different gases such as HCHO,[9] $CO_2$,[13] CO,[14] $CH_3OH$,[15] $H_2$,[16] etc.

$ABO_3$ perovskites are promising candidates for resistive-type gas sensors due to several key factors: (1) the structural stability provided by the abundance of metallic elements in the perovskite composition,[17] (2) the ability to modify the structure and chemical composition through partial substitution of A and/or B cations with aliovalent elements of different sizes and valences,[18,19] (3) the preservation of structural integrity despite deviations from stoichiometry,[20] and (4) their distinctive electronic structure and high electron mobility.[21] In perovskites, oxygen-deficient vacancies are more common than cationic vacancies, likely because anionic vacancies require less energy to form.[22] The presence of both cationic and oxygen vacancies enhances their electrical and redox properties, as well as their catalytic behavior, which significantly impacts gas-sensing capabilities. Their mechanical and thermal stability also makes them suitable for sensing applications over a wide temperature range.

The performance of chemiresistive gas sensors is influenced by environmental factors, such as humidity, operating temperature, and gas concentration. Key parameters include the limit of detection, response/recovery times, sensitivity, selectivity, drift, and reversibility. An ideal sensor exhibits fast response/recovery, high sensitivity and selectivity, and full recovery without drift.[23] Using perovskite oxides for chemiresistive sensors presents challenges due to the high-temperature heat treatment required to achieve a well-defined crystalline phase. However, this process can paradoxically lead to significant grain growth in perovskite oxide nanostructures, reducing the active surface area available for gas interactions and ultimately impairing sensing performance.[24] Additionally, the inherently low surface activity of perovskite oxides has limited their application in chemiresistive sensors. This limitation is largely due to their p-type semiconducting behavior, which is dominated by positive charge carriers. As noted by Hübner et al., p-type oxide sensors typically exhibit a response proportional to the square root of the gas concentration under identical morphological configurations.[25] Despite these challenges, ongoing research efforts aim to overcome these limitations and improve the sensing performance of p-type perovskite oxide-based sensors.

Understanding the fundamental sensing mechanisms and influential factors on sensing performance provides comprehensive knowledge to overcome perovskite oxide gas sensor limitations. In recent years, numerous review articles have explored perovskite oxide-based gas sensors,[26−28] often focusing on specific aspects such as synthesis methods, structural properties, or applications for detection of specific gases. Singh et al.[27] reviewed recent advances in perovskite-based sensors for VOC detection, emphasizing their role in early disease diagnosis. They compared metal halide and metal oxide perovskites, analyzing their sensing mechanisms, structural differences, and synthesis methods. Key factors affecting performance are also discussed. Souri et al.[28] reviewed recent progress in room-temperature perovskite gas sensors, highlighting their high sensitivity, selectivity, and stability. They discussed key factors affecting performance including dopants, oxygen vacancies, and surface morphology. The study emphasizes the importance of understanding sensing mechanisms to advance perovskite-based gas sensors for practical applications.

This review provides a distinct contribution by integrating insights into fundamental sensing mechanisms with advanced material design strategies. This paper emphasizes the role of oxygen vacancies, surface defects, and heterojunctions in enhancing charge carrier dynamics and gas adsorption. Furthermore, we present a comprehensive overview of cutting-edge synthesis techniques, including the use of metal−organic frameworks (MOFs) and other innovative methods, while linking these advancements to their impact on sensor performance. Additionally, this review expands the scope to include a broad range of target gases, such as VOCs, $NO_2$, and $CO_2$, and highlights the interplay between morphology, composition, and functionality. These aspects position this article as a valuable resource for advancing perovskite-based gas sensor research, addressing key gaps in understanding and practical application. It also summarizes current performance metrics and discusses the challenges that need to be addressed while suggesting new directions for future applications.

## 2. CLASSIFICATION OF THE PEROVSKITE OXIDE MATERIALS

Perovskite oxides can be broadly classified into three main categories: simple, double, and layered perovskites. Approximately 90% of metallic elements are known to crystallize in the perovskite structure, as oxides and halides can form various morphologies, including isotropic, anisotropic, and amorphous forms. 1- Simple Perovskites ($ABO_3$): In these structures, the A-site cation is typically a larger alkali, alkaline earth, or rare earth metal coordinating with 12 oxygen atoms. The B-site is a smaller transition metal cation, forming $BO_6$ octahedra that share


https://doi.org/10.1021/acsomega.4c11667
ACS Omega 2025, 10, 13780−13796

corners (Figure 1). This coordination remains stable when the ionic radii of A ($r_A$), B ($r_B$), and O ($r_O$) ions fall within the constraints defined by Goldschmidt tolerance factor, t:[29]

$$t = \frac{r_A + r_O}{\sqrt{2}(r_B + r_O)} \quad (1)$$

A tolerance factor between 0.9-1 is favorable for formation of the stable perovskite structure.[30] The ideal perovskite structure with a cubic system has tolerance *factor of* 1.[31] 2- Double Perovskite Oxides (AA'BB'$O_6$): These structures feature corner-sharing $BO_6$ and B'$O_6$ octahedra, with A and A' positions occupied by alkali, alkaline earth, or rare earth metal cations. The difference in the sizes of the B and B' cations influences the degree of ordering within the structure. Ordering of cations on the A and B sites can significantly alter the physical properties of double perovskites.[32] 3- Layered Perovskite Oxides: These structures are derived from simple perovskites ($ABO_3$) by cutting along the (001) direction and adding extra oxygen layers. They are further categorized into Aurivillius, Ruddlesden–Popper, and Dion-Jacobson oxides depending on the interlayer cations present. The structural diversity and symmetry of perovskite oxides give them unique physicochemical properties, influencing their functionality as gas sensors, which will be discussed in subsequent sections.

## 3. RECENT ADVANCES IN SYNTHESIS AND FABRICATION TECHNIQUES

Perovskite oxide ceramics are synthesized by using various physical and chemical properties inherent to the materials. The conventional ceramic method, which involves solid-state reactions at high temperatures, is commonly employed for producing these materials.[33] However, the traditional ceramic synthesis using solid-state reactions presents some limitations, such as the need for repeated grinding and heating of metal oxides or their salts before calcination.[34] These drawbacks include product inhomogeneity, the presence of defects that can affect luminescence, contamination from grinding and heating, and coarse particles that cannot be used for coatings.[35]

Future research should focus on refining the preparation process to enhance the charge transfer and storage capacity by adjusting the morphology or integrating other materials. Therefore, various preparation methods are detailed to aid in choosing the most suitable approach for different substances. Effective synthesis of perovskite materials with customizable morphologies is crucial for in-depth analysis of their microstructure and electrochemical properties. Different preparation techniques significantly influence the material's size, structural morphology, and electrochemical performance. To address these issues and obtain purer materials, several alternative synthesis techniques have been developed, including coprecipitation,[36] hydrothermal synthesis,[37] solid-state reactions,[38] the Pechini method,[39] sol–gel,[40] microwave synthesis,[14] physical vapor deposition (PVD) methods like laser ablation,[41] wet chemical techniques, and some other methods[42] (Figure 2).

**3.1. Coprecipitation Method.** This technique is commonly used for synthesizing simple oxides like ZnO.[43] It involves precipitation of metal salts by adding a reagent that lowers solubility. Coprecipitation occurs by the simultaneous precipitation of different cations. For uniform product formation, it is essential to control temperature, concentration, pH, and solution homogeneity. Common reagents for precipitation include ammonia, urea, ammonium oxalate, and ammonium carbonate. The resulting oxide compounds, which are insoluble, form through the thermal decomposition of hydroxides or organic/carbonate salts.[44] Coprecipitation due to simplicity, ease of control, cost-effective, and broad variation can be a promising method for synthesis of gas-sensing nanomaterials.[45] Recently, a coprecipitation method was applied for synthesis of Zn-doped $In_2O_3$ with starfish-like dendritic structures and used for triethylamine (TEA) sensing at ppb-level selectively.[46]

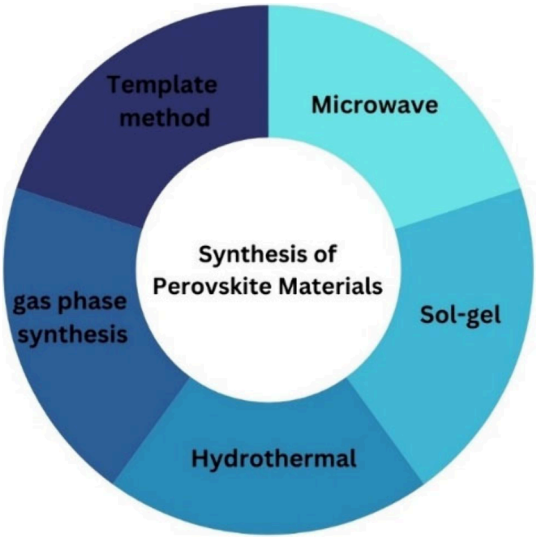


**Figure 2.** Perovskite materials synthesis methods.

**3.2. Solid-State Reactions.** In these reactions, both the starting materials and the final products are solids. Reagents like carbonates, nitrates, or oxides are mixed in stoichiometric ratios[47] and generally without addition of solvents, perovskite materials with large particle size and limited specific surface area provides.[48] For perovskite synthesis, oxides or carbonates of A- and B-site metal ions are combined according to the formula $ABO_3$. This process requires temperatures above two-thirds of the melting point and may last up to 10 h to achieve the desired composition. The materials are ball-milled in isopropanol or acetone, dried at 100 °C, then calcined for 4–8 h at 600 °C with controlled temperature cycles (2 °C/min). Further grinding, sieving, and recalcination at 1300–1600 °C for 5–15 h ensure a single-phase perovskite formation.[49]

**3.3. Hydrothermal Synthesis.** This method involves carrying out reactions in an aqueous solution or suspending the precursors at elevated temperatures and pressure. It is a simple and cost-effective method which allows to produce crystalline powders without calcination[50] with increased chemical reactivity.[51] This method enables control over particle size and shape through temperature, pH, time, and reactant concentration.[52] Recent advancements include synthesizing $NiTiO_3$ perovskite nanoparticles (NPs) at various reaction times, and it was reported that band gap decreases by increasing the reaction time and maximum response to $CO_2$ gas at room temperature (RT) obtained after 24 h reaction time.[53]

**3.4. Gas-Phase Preparations.** This approach is used to deposit perovskite films with specific structures and thicknesses.[54] Techniques vary based on temperature: direct deposition at crystallization temperature, intermediate deposition followed by postannealing (873–1073 K), or deposition at a low substrate temperature followed by high-temperature annealing.[49]


https://doi.org/10.1021/acsomega.4c11667
ACS Omega 2025, 10, 13780–13796

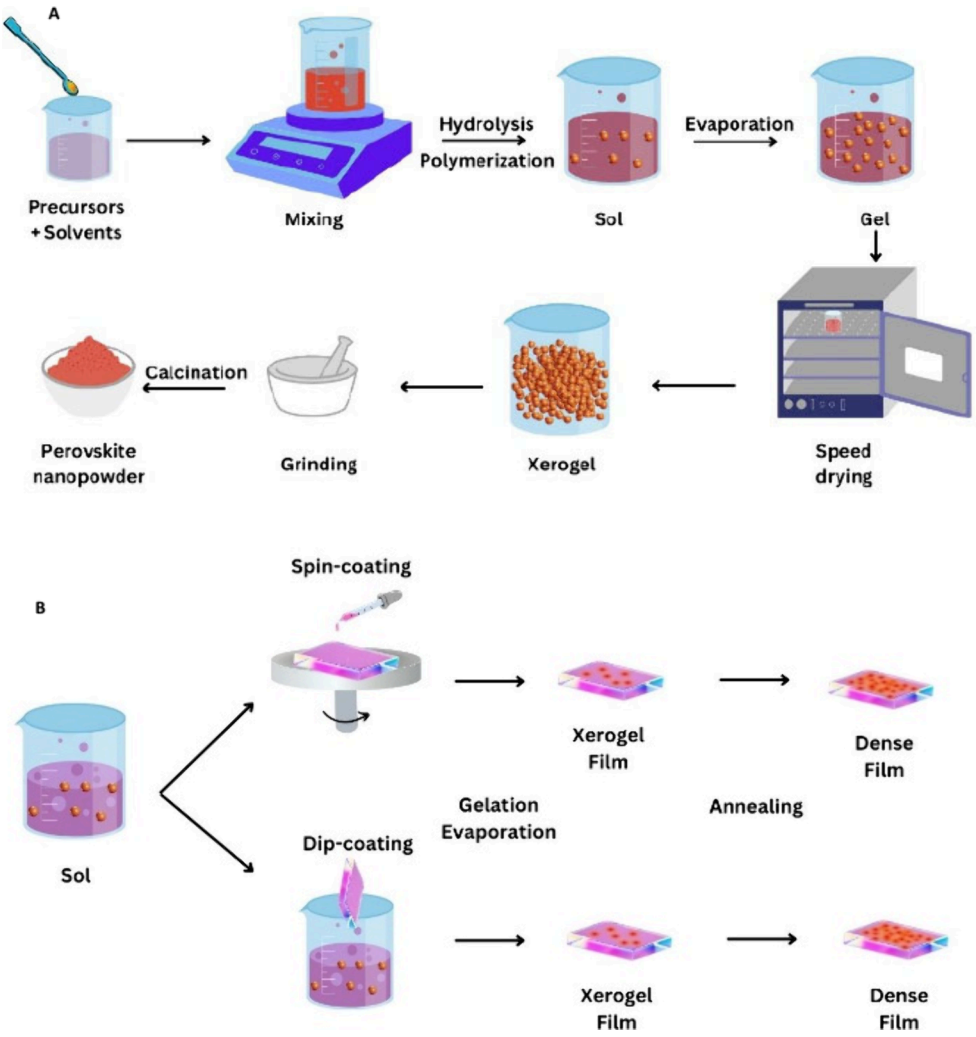


**Figure 3.** A) Schematic illustration of the sol–gel synthesis process and B) thin film processing.

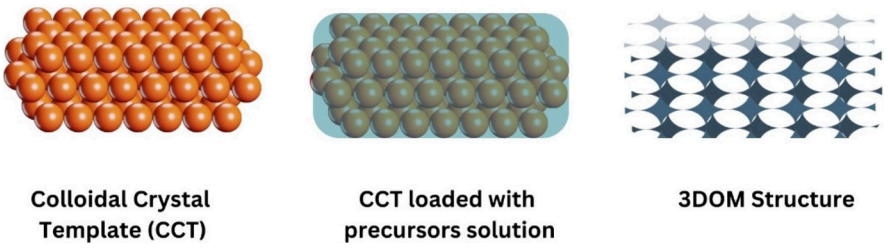


**Figure 4.** Schematic illustration of the colloidal-crystal-template (CCT) synthesis method.

**3.5. Sol–Gel Method.** This technique involves the hydrolysis and poly condensation of metallic alkoxides, which are commercially available for various metals.[55] The sol–gel method used for preparing nanosized materials and thin films allows control of the particle size of the composites, and very pure homogeneous materials and uniform nanomaterials at low temperatures can be obtained.[56] A schematic illustration of the sol–gel synthesis process is represented in Figure 3-A. However, its application is limited by precursor stability and challenges in controlling the composition of complex oxides, also by the requirement of different complexing agents, long reaction times, and special conditions (pH, temperature, etc.).[57,58] Aqueous sol–gel processes often use inorganic salts and carboxylic acids or polyols as chelating agents.[59] A schematic view of the sol–gel process for the development of thin films is shown in Figure 3-B. A sol–gel synthesis of modified $LaCrO_3$ thin film prepared by spin coating represented rapid response and recovery time for CO, $CO_2$, and LPG.[60] Recently sol–gel synthesized CNT-doped $LaFeO_3$ showed superior sensing ability toward LPG gas due to its porous structure and higher surface activity.[61]

**3.6. Microwave Synthesis.** Microwave irradiation offers a time- and energy-efficient alternative for synthesizing perovskite oxides.[62] It can be combined with other techniques such as sol–gel or hydrothermal synthesis to enhance control over stoichiometry and phase formation.[63] Microwave synthesis is particularly effective for synthesizing Pb-containing perovskites due to minimized lead loss.[62] Recently, Gildo-Ortiz et al. employed a simple and economical microwave-assisted solution


https://doi.org/10.1021/acsomega.4c11667
ACS Omega 2025, 10, 13780–13796

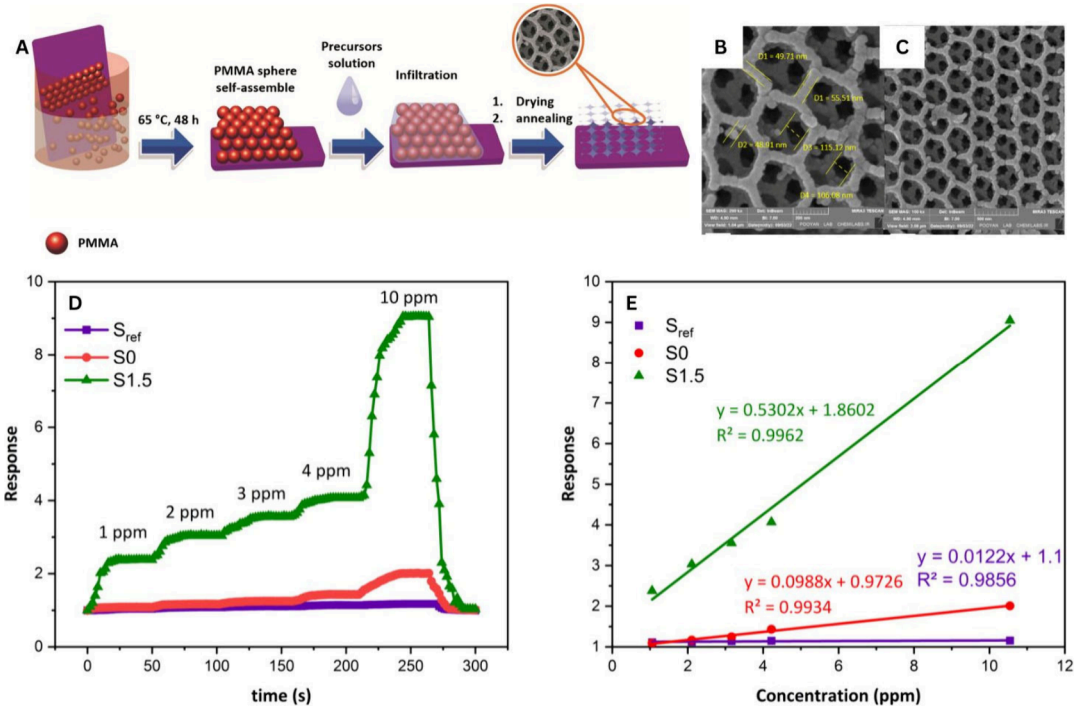


**Figure 5.** A) Schematic illustration of a synthetic process for 3DOM In-doped $SmFeO_3$, B, C) SEM images, and D, E) dynamic response transition of 3DOM In-doped $SmFeO_3$ toward different concentrations of formaldehyde gas. Reproduced with permission from.[9]

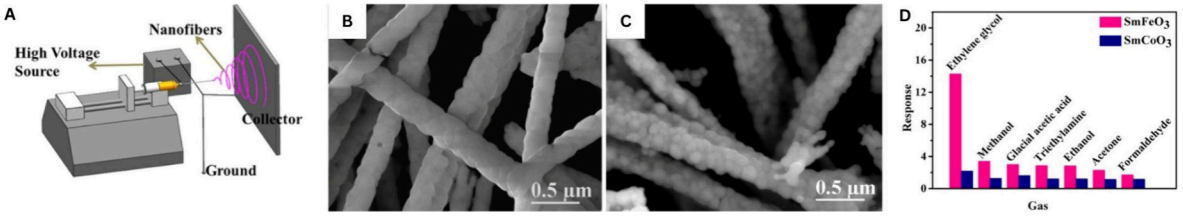


**Figure 6.** A) Schematic illustrations of the electrospinning setup, SEM images of B) $SmFeO_3$ and (C) $SmCoO_3$, and D) selectivity of the samples toward different gases. Reproduced with permission from.[69]

method to produce $LaFeO_3$ nanocrystalline perovskites. As a result, nanomaterials with high sensitivity to CO were obtained at lower temperature in comparison to those from a solid-state synthesis method.[14]

**3.7. Other Synthesis Methods.** The colloidal-crystal-template (CCT) method is another synthesis procedure to prepare nanoporous and three-dimensionally ordered macropore (3DOM) perovskite materials. In this method organic polymer spheres are used as a template to produce pores with different sizes in inorganic materials (Figure 4).[64] Recently, Souri et al. has used poly(methyl methacrylate) (PMMA) for the synthesis of highly sensitive In-doped $SmFeO_3$ for the detection of the formaldehyde gas (Figure 5).[9]

The Pechini Method, also known as the polymeric precursor or mixed liquid method, enables precise control over reaction stoichiometry and provides high reproducibility and homogeneity.[50] This method offers fabrication of uniform, highly pure perovskite materials at low temperature.[65] It involves forming a chelate through the reaction of metal cations with a carboxylic acid, followed by heating a mixture of metal salts, citric acid, and ethylene glycol (80−100 °C) to form a clear solution. Further heating (150−250 °C) induces condensation reactions that lead to a polyester ″resin″ in which metal cations are uniformly distributed.[66] Derakhshi et al. employed Pechini sol−gel method for the synthesis of $LaFe_{0.4}Cu_{0.6}O_3$ perovskites, which results in 6.5 times higher response to 300 ppm ethanol at 300 °C compared to $LaFeO_3$.[67]

Electrospinning is a method used to produce nanofibers with diameters below 100 nm and lengths extending up to several kilometers. This technique employs an electrostatically driven jet of a polymer fluid stream under a high-voltage electric field. Electrospinning has attracted significant interest across numerous fields, such as sensor technology, due to its capability to create continuous fibers with diameters as small as a few nanometers and its adaptability to different compositions, including polymers, polymer blends, polymers embedded with nanoparticles, and metal oxides.[68] Han et al. have studied the gas sensing properties of $SmFeO_3$ and $SmCoO_3$ gas sensors prepared by electrospinning methods toward ethylene glycol at the optimal working temperature of 200 °C.[69] Results have indicated that the $SmFeO_3$ nanofiber showed 6.5 times higher response than $SmCoO_3$ toward 100 ppm ethylene glycol (Figure 6).

Various synthetic methods for perovskite materials, such as hydrothermal, sol−gel, solid-state reaction, microwave-assisted, and combustion techniques, typically require high calcination temperatures (above 800 °C) for several hours to achieve good crystallinity, resulting in larger particle sizes. The summary of


https://doi.org/10.1021/acsomega.4c11667
ACS Omega 2025, 10, 13780−13796

each synthesis method is given in Table 1. Electrodeposition, however, is a simple, safe, controllable, and environmentally friendly method that has been widely employed to prepare perovskite materials under milder conditions.[70,71]

**Table 1. Summary of the pros and cons of different synthesis methods of perovskite materials**

| Synthesis Method | Advantages | Disadvantages |
|---|---|---|
| Solid-State Reaction | - Simple and cost-effective | - High temperature required (~1000−1500 °C) |
| | - Suitable for large-scale production | - Long processing time |
| | - Produces stable crystalline structures | - Poor control over particle size and morphology |
| Sol−Gel Method | - Low-temperature synthesis | - Time-consuming |
| | - Good chemical homogeneity | - Requires organic solvents |
| | - Precise control over composition and morphology | - Risk of impurity incorporation |
| Hydrothermal Synthesis | - Low-temperature process | - Requires high-pressure conditions |
| | - Produces high-purity and crystalline materials | - Limited scalability for industrial applications |
| | - Enables controlled morphology (nanorods, nanospheres) | - Long reaction times |
| Coprecipitation | - Simple and cost-effective | - Requires careful pH control |
| | - Produces homogeneous materials | - Post-treatment needed to enhance crystallinity |
| | - Scalable for large-scale production | - Risk of agglomeration |
| Pechini Method | - Produces fine, uniform powders | - Involves complex organic chemistry |
| | - Good compositional control | - Requires long processing steps |
| | - Lower calcination temperature compared to solid-state synthesis | - Expensive reagents needed |
| Microwave-Assisted Synthesis | - Rapid heating and reaction | - Limited scalability |
| | - Energy-efficient | - Requires special equipment |
| | - Produces small and uniform particles | - Not suitable for all perovskite compositions |
| Electrochemical Deposition | - Precise thickness and composition control | - Limited to thin films |
| | - Low temperature | - Requires conductive substrates |
| | - Environmentally friendly | - Slow deposition rate |

Electrochemical methods, such as anodic oxidation, cathodic reduction, and alternating current synthesis, are used to fabricate perovskite oxide thin films. These methods offer advantages like precise control over composition, lower synthesis temperatures compared to traditional solid-state reactions, and cost-effectiveness.[72] For example, researchers have successfully synthesized $LaMnO_3$,[73] $La_{1-x}Sr_xMnO_3$,[74] and $LaCoO_3$[75] perovskites using anodic oxidation. This process involves electrochemically incorporating $La^{3+}$ ions into metal oxyhydroxide films, followed by thermal treatment to achieve the perovskite phase. However, challenges include controlling the incorporation of $La^{3+}$ ions and ensuring uniform phase formation.[72]

Cathodic reduction methods have also been employed, where metal cations are codeposited from a mixed nitrate solution, forming hydroxide precursors that convert into perovskite oxides after heat treatment. This method facilitates better control over composition and enables the synthesis of perovskites like $LaMO_3$ (M = Al, Mn, Fe, Co, Ni).[70]

Additionally, chemically assisted electrodeposition (CAED) has been introduced as a novel technique for fabricating perovskite electrodes with a nanostructured morphology. This method combines electrodeposition with chemical precipitation, allowing the formation of highly porous, catalytically active electrodes.[72]

## 4. MECHANISMS OF GAS SENSING IN PEROVSKITE-BASED SENSORS

The widely recognized gas sensing mechanism for resistive-type gas sensors, including perovskite-based ones, involves changes in the material's conductivity due to the desorption and adsorption of gas molecules on the surface of the probing material when exposed to target gases (Figure 7). This mechanism is influenced by the properties of both the sensor material and the target gases.[28] In air, oxygen molecules adsorb onto the surface of semiconductor perovskites, where surface reactions occur between the target gases and the chemisorbed oxygen species (such as $O^-$, $O_2^-$, and $O^{2-}$). These oxygen species form by extracting surface electrons, with the specific species depending on the temperature range. The general reactions include:[3,76]

$$O_{2(gas)} \rightarrow O_{2(ads)} \quad (2)$$

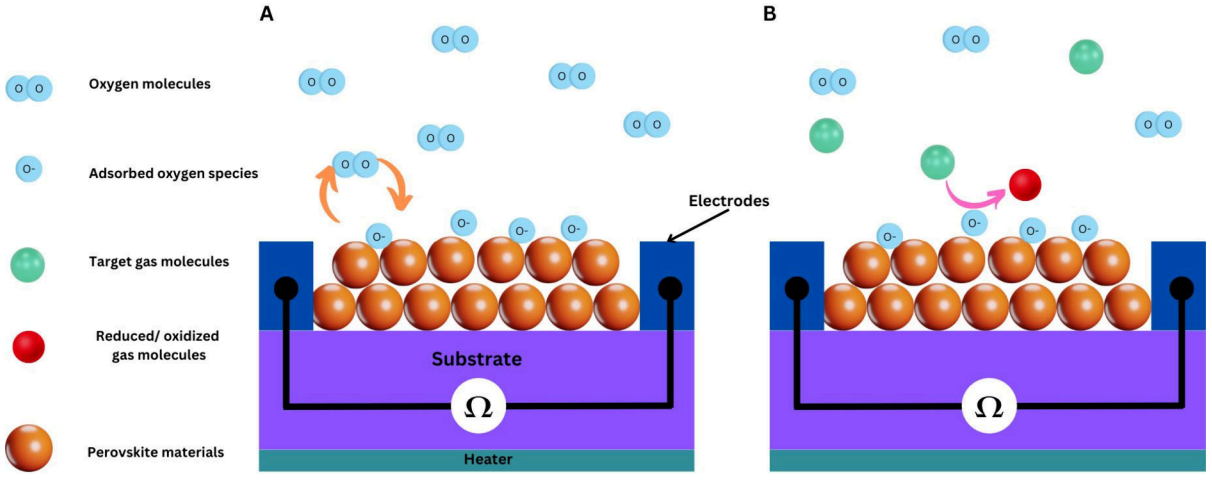


**Figure 7.** Schematic of the gas-sensing behavior of perovskite oxide materials.



https://doi.org/10.1021/acsomega.4c11667
ACS Omega 2025, 10, 13780−13796

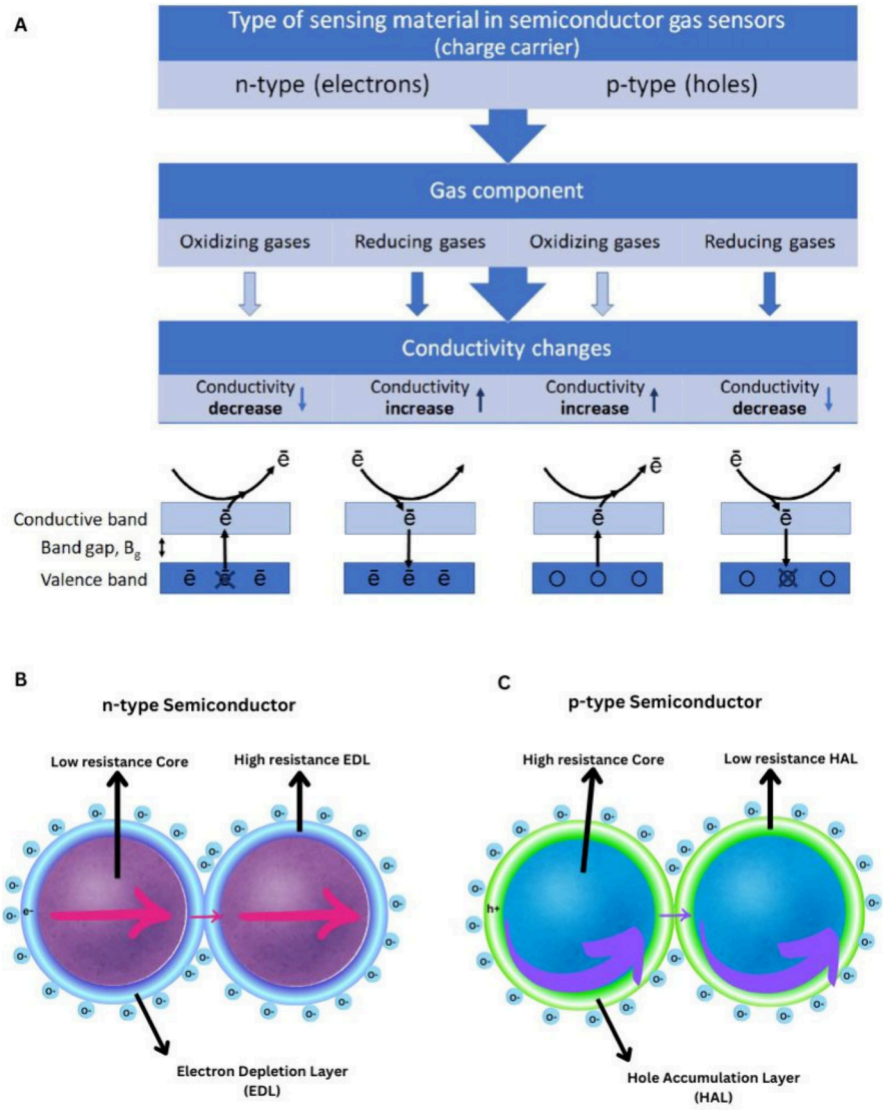


**Figure 8.** A) Description of the gas-sensing mechanism and the conduction model toward different gases. Reproduced with permission from.[26] B,C) Charge carrier mechanism in different types of semiconductors.

$$O_{2(ads)} + e^- \rightarrow O^-_{2(ads)} \quad (T < 300\,^\circ\mathrm{C}) \tag{3}$$

$$O^-_{2(ads)} + e^- \rightarrow 2O^-_{(ads)} \quad (100\,^\circ\mathrm{C} < T < 300\,^\circ\mathrm{C}) \tag{4}$$

$$O^-_{(ads)} + e^- \rightarrow O^{2-}_{(ads)} \quad (T > 300\,^\circ\mathrm{C}) \tag{5}$$

In n-type semiconductors, where electrons are the main charge carriers, the formation of chemisorbed oxygen ions reduces the electron density, creating an electron depletion layer that raises the resistance. Conversely, in p-type semiconductors, where holes are the primary charge carriers, the adsorption of oxygen ions produces a hole accumulation layer near the surface and an insulating core, which increases conductivity by boosting hole concentration (Figure 8).

When p-type perovskites encounter reducing gases (e.g., acetone, ethanol, acetaldehyde, formaldehyde, methane, or hydrogen sulfide), the reducing gas reacts with adsorbed oxygen ions, releasing trapped electrons and neutralizing holes. This lowers the charge carrier concentration, thereby increasing the resistance. For oxidizing gases (e.g., nitrogen dioxide, hydrogen peroxide, ozone, carbon dioxide, sulfur dioxide), the interaction increases hole concentration and decreases resistance.[77]

In n-type perovskites, interaction with reducing gases, which typically compensate for oxygen vacancy deficiencies, results in higher electron concentration and lower resistance, as electrons are returned into the conduction band by the ionized oxygen species. In oxidizing environments, the target gas reduce by taking electrons from the conduction band, leading to the resistance of n-type perovskites increases.[78,79]

## 5. OPTIMIZATION OF THE GAS-SENSING PROPERTIES OF THE PEROVSKITE MATERIALS

**5.1. Tailoring the Chemical Composition of the Perovskite Materials.** Typically, perovskite oxide-based sensors with p-type properties exhibit a mechanism of resistance change that is the opposite of that of n-type semiconductor sensors, leading to a reduced response in the environment of volatile organic compounds (VOCs) or sulfuric compounds (VSCs). To overcome this limitation, many studies have focused on various strategies such as doping at the A and B sites within the perovskite structure, incorporating noble metal catalysts, and applying nanoengineering techniques to increase the surface area and porosity.


https://doi.org/10.1021/acsomega.4c11667
ACS Omega 2025, 10, 13780−13796

The sensing properties of $ABO_3$ perovskites can be significantly improved by incorporating various cationic elements into the A and B sites of the structure. Doping these materials enhances their selectivity and sensitivity to volatile organic compounds (VOCs) and reduces both response and recovery times. Liu et al. doped yttrium (Y) into $LaFeO_3$ (LFO) at different concentrations, with 0.8 mol % Y showing the highest sensing response. The incorporation of Y increases the number of free electrons and surface charge exchange, leading to more active sites for gas adsorption and stronger gas molecule interaction.[80] Qin et al. replaced a low-valence B-site cation with phosphorus ($P^{5+}$), which substituted part of the B−O octahedra in the perovskite structure with P−O tetrahedra, creating oxygen vacancies. This doping significantly enhanced the sensor's sensitivity to acetone at 180 °C, although excessive P doping led to reduced performance due to increased resistance in the presence of acetone, a reducing gas.[81] Additionally, doping with magnesium ($Mg^{2+}$) improved LFO's performance for methanol detection, as $Mg^{2+}$ creates oxygen vacancies, enhancing gas sensitivity by facilitating oxygen absorption.[82]

Furthermore, both A-site and B-site doping have been explored for improving gas sensing in perovskites. For example, Liu et al. found that doping $Y^{3+}$ in $LaMnO_3$ enhanced acetone sensing by increasing the number of adsorbed oxygen species and promoting the formation of $Mn^{4+}$ ions.[83] Similarly, doping calcium ($Ca^{2+}$) in $GdFeO_3$, a p-type semiconductor, generated oxygen vacancies and promoted hole production, improving sensitivity and selectivity for methanol.[84]

However, there remains a considerable need for more efficient and effective processing approaches to improve the practical use of perovskite oxide-based sensors. Modifying the composition of a material, either partially or completely, can be a potential strategy to boost the gas response of p-type materials.

The role of defects in semiconductors has been extensively studied, and various techniques such as hydrothermal methods, surface engineering, and ion-beam irradiation have been used to create and understand these defects.[85−89] Defects, particularly voids or missing lattice sites, are significant, as they influence the sensor response. These defects, which can be shallow or deep donors depending on their energetics, impact gas sensing by altering the electrical properties of the materials. Specifically, deficiencies at the A- or B-sites and oxygen vacancies in perovskite oxide-based materials are known to influence the adsorption and dissociation energy between oxygen species and target analytes, thereby enhancing selectivity. Oxygen vacancy defects (VO··, O, and $O^{2-}$) play crucial roles in gas sensor response, and the sensor's electrical resistance is influenced by the target gas's partial pressure and defect concentration.[90] Recently, investigation on the freeze-dried assisted sol−gel synthesized $SmFeO_3$ revealed a superior acetylene sensing ability that related to the rich surface oxygen vacancies.[91]

For example, in perovskite materials, defects such as surface vacancies created during the synthesis process can lead to lower conductivity, but these can be passivated by adsorbing target vapors like ethanol. The adsorbed vapors help release trapped electrons, boosting the material's conductivity. Surface defects, which act as a route for ion diffusion, can be detrimental, leading to ion migration and reduced performance over time.[92]

Further, in the case of multiferroic sensors, such as $BiFeO_3$ (BFO), defects at domain walls, including $Fe^{4+}$ ions and Bi vacancies, impact the sensor's behavior. These defects increase the presence of adsorbed oxygen species, which can reduce response times under thermal excitation. Magnetic excitation can further activate these adsorbed oxygen species, reducing the ideal operating temperature and speeding recovery times. This suggests that while surface defects may limit performance in optical applications, they are advantageous for humidity and gas sensing due to their ability to facilitate oxygen adsorption and charge transfer.[93] In conclusion, defects play a pivotal role in enhancing or hindering the performance of gas sensors, with specific defects like oxygen vacancies and surface defects contributing to improved sensitivity and faster response times when managed properly.

Additionally, incorporating perovskite oxide with spillover effects into the sensing layer can enhance the quantity of oxygen species, which provides higher reaction sites for molecules of the target gases.

These studies illustrate how doping and defects in $ABO_3$ perovskites, such as the creation of oxygen vacancies and the introduction of new active sites, significantly enhance their gas sensing performance.

**5.2. Tuning the Morphology of the Perovskite Materials.** The morphology of materials plays a crucial role in enhancing the gas-sensing performance, especially for volatile organic compounds (VOCs) at various concentrations and temperatures. Nanomaterials, with their high surface-to-volume ratios, exhibit superior sensing effects. For thin-film-based sensors, the grain size significantly influences sensor properties, as smaller grains (less than twice the Debye length) lead to better charge transfer, improving sensitivity.[94] Using a porous structure with a large surface area is a widely used and effective approach to enhancing gas sensing performance. Porous materials, due to their special structural and morphological characteristics, have been extensively studied in this regard.[95] Among the various synthesis techniques, the template method has proven to be highly effective for producing porous materials. Recently, metal−organic frameworks (MOFs) have gained significant attention as an innovative template for fabricating porous nanomaterials.[96] MOFs themselves are porous, multifunctional materials composed of metal clusters interconnected by functional organic ligands.[97] Their exceptional features, including uniform porous structure with high surface area, make them suitable for different applications, including catalysis,[98] drug delivery,[99] gas storage, separation, and gas sensing.[100]

Additionally, MOFs offer a unique pathway for synthesizing porous perovskite structured nanomaterials. Modified $La_{0.8}Ca_{0.2}Fe_{0.98}Pt_{0.02}O_3$ gas sensor using (MOF)-derived $\alpha$-$Fe_2O_3$ nanoparticles demonstrated exceptional chemoresistive performance for acetone detection at 250 °C.[101] Hollow box-shaped CNT@$ZnSnO_3$ synthesized by a hydrothermal method and Zn-MOF (ZIF-8) exhibited excellent ethanol sensing performance due to large specific surface area.[102]

Materials with varying morphologies, such as nanofibers, thick films, and powders, show different gas sensing performances. For example, $LaFeO_3$ (LFO) in the nanofiber form detected ethanol at a lower temperature but had slower response times compared to the thicker film version, which exhibited higher sensitivity despite slower recovery times. The material's surface area, pore size, and crystallite structure all influence these outcomes.[103,104] Phan et al. reported that $LaFeO_3$ indicates different ethanol-sensing properties depending on the morphological structure. They have synthesized $LaFeO_3$ with a hollow core and porous shell structure using a surfactant-assisted hydrothermal method. $LaFeO_3$ with porous structure has shown better selectivity and higher sensitivity in comparison to a bulk structure.[105] A study explored hierarchically porous $LaFeO_3$


https://doi.org/10.1021/acsomega.4c11667
ACS Omega 2025, 10, 13780−13796

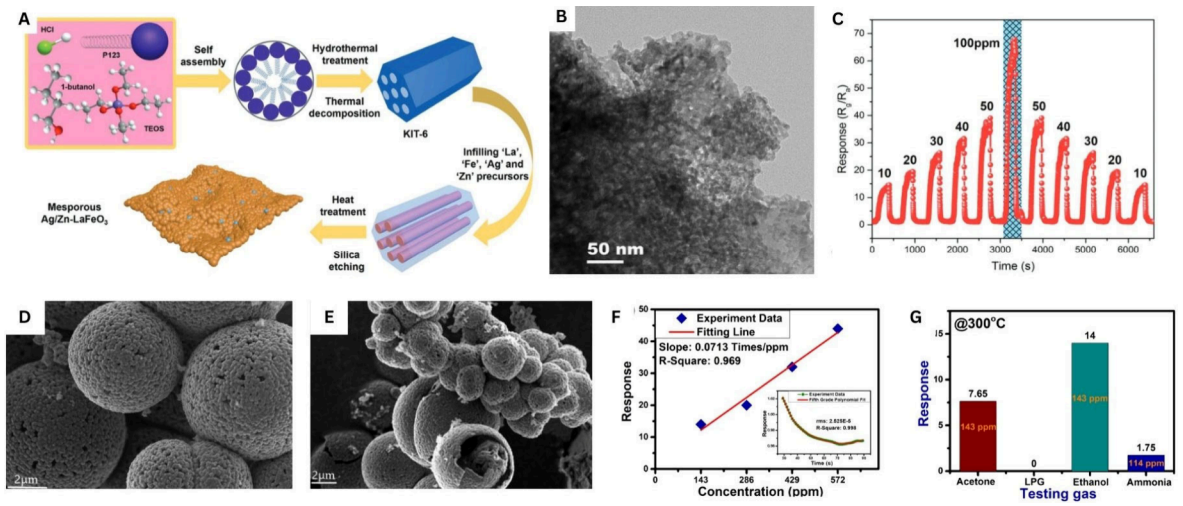


**Figure 9.** A) Schematic diagram of the synthesis process by hard template of KIT-6, B) TEM image, and C) dynamic response of mesoporous Ag/Zn−$LaFeO_3$ nanocomposites toward ethanol gas and toward different gases. Reproduced with permission from.[106] D, E) SEM images and F, G) ethanol sensing performance of hollow $LaFeO_3$ toward different gases. Reproduced with permission from.[105]

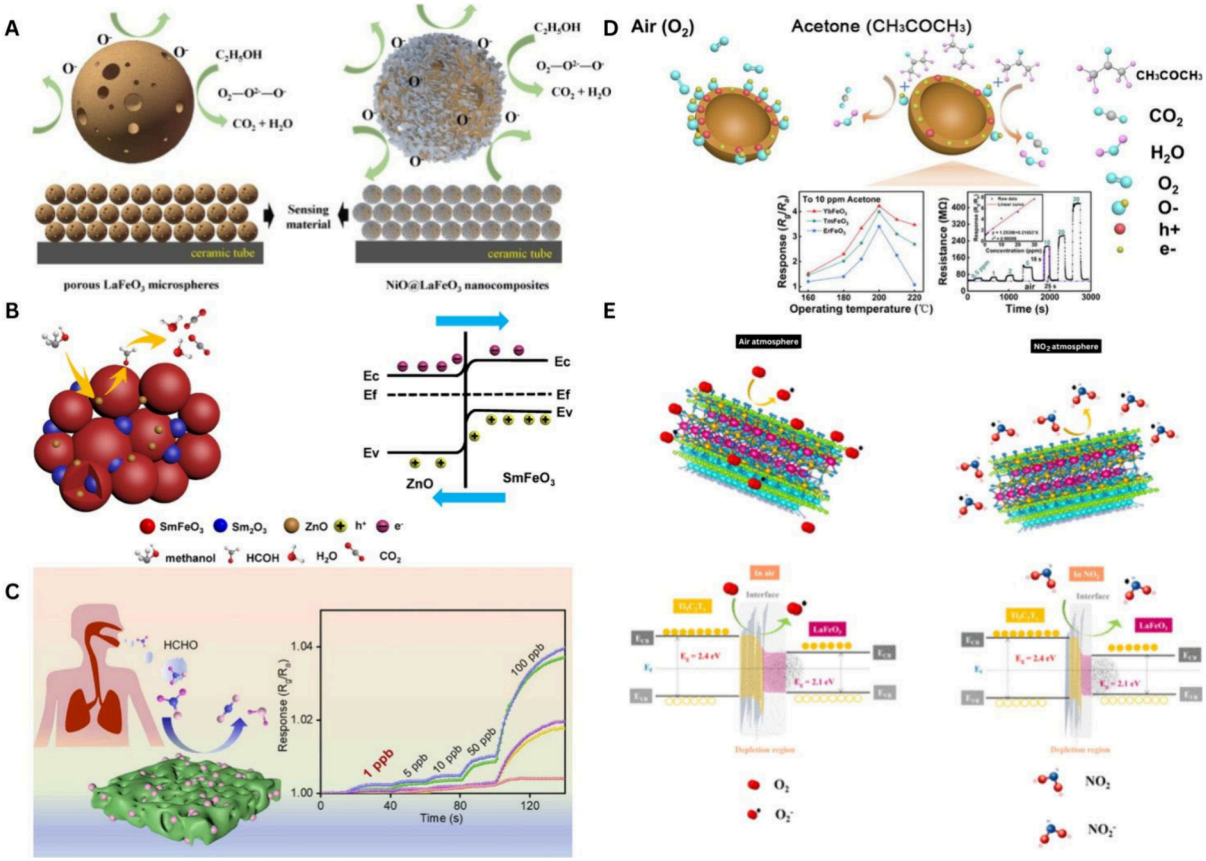


**Figure 10.** Gas sensing properties of the perovskite materials A) ethanol gas sensor based on $LaFeO_3$ microspheres decorated with NiO nanosheets,[114] B) methanol gas sensor based on $Sm_2O_3$/ZnO/$SmFeO_3$ microspheres,[116] C) formaldehyde gas sensor based on In-doped $LaFeO_3$ porous structure,[120] D) acetone gas sensor based on porous $YbFeO_3$ nanocrystalline,[124] and E) $NO_2$ gas sensor based on cotton-modified $LaFeO_3$/MXene composites.[137] All figures are reproduced with permission.

synthesized using a cost-effective and scalable method. By optimizing the quantity of the structuring agent F108 and the calcination temperature, the gas-sensing performance was significantly improved. The $LaFeO_3$ prepared with 0.5 g of F108 exhibited the best response, achieving a sensitivity of 116 to 50 ppm formaldehyde at 125 °C with a trace detection limit as low as 50 ppb. The enhanced performance was attributed to the material's hierarchical porous structure, which provides a high surface area and large pore volume.[76] This approach highlights the importance of morphological tuning for achieving superior gas-sensing properties and positions $LaFeO_3$ as a promising material for accurate and noninvasive formaldehyde detection.

The mesoporous Ag/Zn−$LaFeO_3$ nanocomposite synthesized through a facile nanocasting technique using silica hard


https://doi.org/10.1021/acsomega.4c11667
ACS Omega 2025, 10, 13780−13796

template KIT-6 using KIT-6 in a sol−gel route is showed high sensing performance toward ethanol at the low temperature of 55 °C. This superior functionality is related to the high surface area and the catalyst behavior of $Zn^{2+}$ at the surface of the sensing materials (Figure 9-A-C).[106] Phan et al. synthesized hollow $LaFeO_3$ (LFO-HS) using a hydrothermal method, with cetyltrimethylammonium bromide (CTAB) playing a crucial role in shaping the particle morphology. The presence of CTAB resulted in a hollow, porous structure with a large surface area, enhancing the gas sensing performance. The LFO-HS-based sensor demonstrated a high resistance, making it suitable for low-power applications. Optimal performance was achieved with a 6-layer LFO-HS sensor at 300 °C, showing strong selectivity for ethanol over acetone, LPG, and ammonia. It exhibited a linear response with an ultralow ethanol detection limit of 1 ppb. Compared to bulk LFO synthesized via a solid-state reaction, the hollow structure significantly improved sensitivity due to differences in structural and microstructural properties. These findings highlight the effect of morphology in the sensing performance of $LaFeO_3$ (Figure 9-D-G).[105]

## 6. GAS-SENSING PROPERTIES OF PEROVSKITE MATERIALS

**6.1. VOCs Sensing Properties.** The several hazards of the volatile organic compound (VOC) gases to human health have been studied previously;[107,108] also it has been shown that detection of them in human breath plays a crucial role for the early stage detection of various diseases like cancer, renal failure, etc.[109−111] Recently, perovskite materials have offered excellent performance for detection of VOC gases accurately, with short response/recovery time and high sensitivity and selectivity, due to their special crystalline structures and optoelectronic properties.[112]

Chen et al. synthesized $SmFe_{1-x}Ni_xO_3$ nanocrystalline materials with an orthogonal perovskite structure via a sol−gel method. It was observed that increasing nickel (Ni) doping resulted in a reduced unit cell volume and average crystallite size. Sensors made from $SmFe_{1-x}Ni_xO_3$ demonstrated improved conductivity and lower optimal working temperatures compared to $SmFeO_3$. At low Ni doping levels ($x \leq 0.05$), the sensors exhibited enhanced sensing performance, attributed to accelerated catalytic oxidation reactions of ethanol on the surface of the material due to Ni incorporation. For example, the $SmFe_{0.95}Ni_{0.05}O_3$ sensor achieved a response of 57.8 to 500 ppm ethanol at 260 °C, with response and recovery times of 30 and 50 s, respectively. This improved response was associated with the smaller particle size and increased specific surface area induced by Ni doping, which facilitated the adsorption and reaction of oxygen species with ethanol, releasing electrons and enhancing resistance change. However, at higher Ni doping levels ($x > 0.05$), the sensing performance declined, potentially due to the diminished role of $Fe^{3+}$ ions at the B site, which is critical to the sensing mechanism. Additionally, Ni doping reduced the optimal operating temperature of the sensors, likely by lowering the adsorption activation energy of the material.[113]

Hao et al. synthesized porous $LaFeO_3$ microspheres decorated with NiO nanosheets by using a hydrothermal method, forming a p-p heterojunction. The uniform NiO nanosheets enhanced the gas interaction surface, significantly improving ethanol sensing performance with high sensitivity, selectivity, and fast response/recovery times. The hierarchical structure and heterointerfaces facilitated oxygen adsorption, making NiO@$LaFeO_3$ a promising material for ethanol detection and offering valuable insights for designing advanced gas sensors (Figure 10-A).[114]

A recent study focused on the preparation of $LaFeO_3/In_2O_3$ composites through hydrothermal methods and analyzed their microstructures and crystal properties. The ethanol sensitivity tests revealed that the $LaFeO_3/In_2O_3$ composite gas sensor exhibited superior performance compared to pure $In_2O_3$. Further calculations and analysis using the first-principles method revealed that $LaFeO_3$ improves the performance of the $In_2O_3$ sensor by increasing oxygen adsorption, creating a heterojunction with unique Fermi level effects, and catalyzing redox reactions. These factors collectively contribute to the enhanced sensitivity of the $LaFeO_3/In_2O_3$ composite sensor.[115]

A recent study developed an Ag-doped double perovskite $LaFe_{1-3}Sn_xO_3$ (Ag-LFSO) nanocomposite using a sol−gel-assisted microwave chemical synthesis method. This composite demonstrated both fast response and good selectivity for methanol detection. The Ag-LFSO sensor exhibited a response of 51.94 to 5 ppm of methanol at 99 °C, which is approximately six times higher than that of the pure $LaFeO_3$ sensor. The enhanced response and selectivity were attributed to the substitution of $Sn^{2+}$ in the $Fe^{3+}$ position, which altered the carrier concentration and oxygen adsorption in $LaFeO_3$. Additionally, the introduction of Ag doping catalyzed surface reactions and created electron defects on the material's surface, improving its electrical conductivity and oxygen adsorption capabilities.[15]

Li et al. developed $Sm_2O_3/ZnO/SmFeO_3$ microspheres using a hydrothermal-microwave method for methanol sensing. The sensor, optimized at a 24h hydrothermal time, exhibited a high response of 119.8 to 5 ppm of methanol at 195 °C, with excellent stability over 30 days in humid conditions. Even at 1 ppm, the response remained strong, demonstrating the material's potential for methanol gas detection (Figure 10-B).[116]

The formaldehyde sensing ability of $LaFeO_3$ has been widely investigated. However, several disadvantages need to be improved to achieve high sensitivity, selectivity, and reduced response/recovery times. Porous Pt-decorated $LaFeO_3$ has been synthesized that represented 2.5 times higher response, better selectivity, and shorter response/recovery times than the pristine material at the low sensing temperature of 125 °C. This improvement is attributed to the porous structure and the increased concentration of the adsorbed oxygen.[117]

Dash et al. have reported that a synergistic effect of reduced graphene oxide (rGO) and $LaFeO_3$ improved the sensing properties of the $LaFeO_3$ gas sensor. Adsorption of formaldehyde molecules was facilitated owing to the large surface area of the rGO, while $LaFeO_3$ represented the catalytic effect for the oxidation of formaldehyde.[118]

Rapid detection of formaldehyde using $YFeO_3$ has been studied by Xukeer et al. The sensor exhibited ultrafast response-recovery times of about 6.3 s/0.9 s due to a uniform hierarchical structure and high oxygen vacancies concentration.[119] Xiao et al. synthesized In-doped $LaFeO_3$ via a sol−gel method to enhance formaldehyde sensing. The sensor showed a high response of 122 at 125 °C toward 100 ppm and detected concentrations as low as 1 ppb. Improved performance was attributed to increased surface area, oxygen vacancies, and lower adsorption energy, making it a promising material for real-time formaldehyde detection (Figure 10-C).[120]

Bing Li et al. investigated $Sm^{3+}$-doped $NdFeO_3$ (Sm-NFO), synthesized via a one-step hydrothermal method, and demonstrated that $Sm^{3+}$ doping significantly enhances the


https://doi.org/10.1021/acsomega.4c11667
ACS Omega 2025, 10, 13780−13796

Table 2. VOCs sensing properties of the perovskite materials

| Material | Synthesize method | Target gas | Operating temp. | concentration | response | Detection limit | ref. |
|---|---|---|---|---|---|---|---|
| $SmFe_{0.95}Ni_{0.05}O_3$ | sol−gel citric | Ethanol | 260 °C | 500 ppm | 57.8 | | 113 |
| NiO@$LaFeO_3$ | hydrothermal | Ethanol | 125 °C | 100 ppm | 122 | 1 ppb | 114 |
| $LaFeO_3/In_2O_3$ | hydrothermal | Ethanol | 220 °C | 100 ppm | 147 | 50 ppb | 115 |
| Ag-$LaFe_{1-x}Sn_xO_3$ | microwave assisted sol−gel | Methanol | 99 °C | 5 ppm | 51.94 | | 15 |
| $Sm_2O_3$/ZnO/$SmFeO_3$ | hydrothermal-microwave | Methanol | 195 °C | 5 ppm | 119.8 | | 116 |
| 1%Pt-$LaFeO_3$ | sol−gel | Formaldehyde | 125 °C | 100 ppm | 144 | 10 ppb | 117 |
| rGO-$LaFeO_3$ | sol−gel | Formaldehyde | 260 °C | 1 ppm | 15 | 19 ppb | 118 |
| $YFeO_3$ | hydrothermal | Formaldehyde | Room temp. | 100 ppm | 318 | | 119 |
| 1.5 at%In- $LaFeO_3$ | sol−gel | Formaldehyde | 125 °C | 100 ppm | 122 | 1 ppb | 120 |
| 1%Sm-$NdFeO_3$ | hydrothermal | Formaldehyde | 210 °C | 100 ppm | 18 | | 121 |
| CNT/Ag-$LaFeO_3$ | microwave assisted sol−gel | Acetone | 86 °C | 5 ppm | 59 | | 123 |
| $YbFeO_3$ | sol−gel | Acetone | 200 °C | 10 ppm | ∼4 | 500 ppb | 124 |
| 10 wt % $TiO_2$−$LaFeO_3$ | sol−gel | Acetone | 144 °C | 100 ppm | 37.3 | | 125 |
| $La_2O_3/LaFeO_3$ | hydrothermal | Acetone | 200 °C | 100 ppm | 41.9 | 500 ppb | 126 |

material's sensitivity and selectivity for formaldehyde detection. The enhanced sensitivity was attributed to morphological changes induced by $Sm^{3+}$ doping, which resulted in a lamellar structure that increased the number of active sites for gas adsorption and improved gas diffusion. Furthermore, the doping process introduced oxygen vacancies and lattice defects, boosting chemisorbed oxygen concentrations and creating additional activation sites for gas sensing. The smaller ionic radius of $Sm^{3+}$ also narrowed the optical bandgap and enhanced electron transport by suppressing electron−hole recombination. These combined effects improved the material's selective adsorption and overall sensing performance, making $Sm^{3+}$ doped $NdFeO_3$ a promising candidate for formaldehyde detection.[121]

Molecularly imprinted polymers (MIPs) are highly selective materials for VOC sensing, as they recognize target molecules based on both their functional groups and specific shapes. MIPs are synthesized by polymerizing functional monomers and a cross-linking agent around a target molecule (template). After the template's removal, cavities matching the target's shape and functionality remain. These cavities allow MIPs to selectively rebind the target molecule upon exposure to a gas mixture. For VOCs like ethanol, toluene, and xylene, MIPs exhibit strong selectivity and significant changes in conductivity upon target binding, making them effective for VOC detection.[122] Rong et al. have employed a composite of Ag-$LaFeO_3$ molecular imprinted polymers and carbon nanotubes for sensitive detection of acetone at the low operating temperature of 86 °C.[123]

Meng et al. studied the selection of a suitable lanthanide that can enhance the gas sensing properties of the $LnFeO_3$ gas sensors. They have mentioned that $YbFeO_3$ represented superior gas sensing ability toward acetone with a low detection limit of 500 ppb. They have concluded that the enhanced gas-sensing performance is mainly related to the low binding energy of the Yb−O bond (Figure 10-D).[124]

A recent study aimed to improve the acetone sensing performance of the sol−gel synthesized $LaFeO_3$ nanoparticles for breath analysis by incorporating commercial rutile $TiO_2$ nanomaterials. The $TiO_2$−$LaFeO_3$ nanocomposites showed enhanced surface reactivity, higher specific surface areas, and more concentration of oxygen vacancy in comparison to pure $LaFeO_3$ nanoparticles. The addition of $TiO_2$ by formation of p-n heterojunctions improved the regulation of acetone molecules and carrier conduction within the nanocomposites. As a result, the nanocomposites showed better acetone sensing performance, improved selectivity, and lower response/recovery times.[125]

Wu et al. have studied mesoporous p-p heterostructure composites of $La_2O_3/LaFeO_3$. The in situ formation of p-p heterojunctions effectively tailors charge carrier concentrations and modifies the energy band structure, enhancing sensing performance. Additionally, the inclusion of La, known for its high catalytic activity, promotes gas sensing reactivity and generates abundant lattice oxygen defects. Consequently, the mesoporous $La_2O_3/LaFeO_3$-based gas sensor exhibited high sensitivity, rapid response and recovery times (9 s/15 s to 100 ppm acetone), excellent selectivity, and a low detection limit (500 ppb) at an operating temperature of 200 °C. In contrast, the acetone sensing performance of the $LaFeO_3$-based sensor alone was comparatively poor. This study offers a straightforward strategy to enhance the chemiresistive sensing performance of $ABO_3$ perovskites.[126] The results obtained for the VOCs sensing properties of the perovskite materials have been summarized in Table 2.

**6.2. $CO_2$ Sensing Properties.** Because of the weak oxidizing and reducing properties of carbon dioxide ($CO_2$), only a limited number of materials are suitable for the development of the $CO_2$ resistive gas sensors. $LaFeO_3$ has demonstrated $CO_2$ sensing capabilities. $LaFeO_3$ nanocrystalline powders, prepared using a sol−gel method, have shown notable $CO_2$ sensing capabilities. First-principles calculations suggest that $CO_2$ molecules donate electrons to the $LaFeO_3$ surface preadsorbed with oxygen.[127] To improve its performance, researchers employed a Co doping strategy. They synthesized $LaFeO_3$ and $LaCo_{0.1}Fe_{0.9}O_3$ nanomaterials via a sol−gel method and used them as gas sensors.[13] The results revealed that the $LaCo_{0.1}Fe_{0.9}O_3$ sensor exhibited a superior $CO_2$ sensing performance compared to the $LaFeO_3$ sensor. It can detect $CO_2$ at the wide range of 25−10,000 ppm, rapid response and recovery times (6/42 s), and higher sensitivity (6.69% response to 1% of $CO_2$) at an optimal operating temperature of 220 °C under relative humidity of 51.9%. Characterization and theoretical analysis suggested that the enhanced performance of the $LaCo_{0.1}Fe_{0.9}O_3$ sensor was primarily related to the increased oxygen vacancies and higher adsorption energy introduced by Co doping. Nanoparticles of $La_{1-x}FeO_{3-\delta}$ with A-site deficiencies were synthesized via flame spray pyrolysis (FSP) and evaluated for their $CO_2$ sensing performance in gas mixtures containing 5%−15% $CO_2$. The results indicated that


https://doi.org/10.1021/acsomega.4c11667
ACS Omega 2025, 10, 13780−13796

Table 3. $CO_2$ sensing properties of the perovskite materials

| material | Synthesize method | Operating temp. | $CO_2$ concentration | Response | ref. |
|---|---|---|---|---|---|
| $LaFeO_3$ | sol−gel | 300 °C | 2000 ppm | 2.19 | 127 |
| $LaCo_{0.1}Fe_{0.9}O_3$ | sol−gel | 220 °C | 1% | 6.69% | 13 |
| $La_{0.95}FeO_{3-\delta}$ | flame spray pyrolysis | | 15% | 3.38 | 128 |
| $BaTiO_3$ | coprecipitation | | 50 ppm | 63% | 129 |
| CaO-$BaTiO_3$ | solution impregnation | 160 °C | 1000 ppm | 65% | 130 |
| Co-doped $PrFeO_3$ | sol−gel autocombustion | Room temp. | 500 ppm | | 131 |

Table 4. $NO_2$ sensing properties of the perovskite materials

| material | Synthesize method | Operating temp. | $NO_2$ concentration | Response | ref. |
|---|---|---|---|---|---|
| $LnFeO_3$ | thermal decomposition | 300 °C | 10 ppm | | 132 |
| $SmFeO_3$ | MOF self-templated precipitation process | 200 °C | 200 ppb | 10.2 | 133 |
| GO/$SrTiO_3$ | Modified Hammer's method | 100 °C | 1 ppm | 3.2 | 134 |
| Sr-$BaTiO_3$ | hydrothermal | room temperature | 1000 ppm | 88 | 135 |
| $LaFeO_3$ | radio frequency magnetron sputtering | room temperature | 1 ppm | 29.6 | 136 |

the sensor performance was strongly influenced by the degree of A-site deficiency. Among the tested compositions (x = 0, 0.02, 0.05, 0.07, and 0.1), the $La_{0.95}FeO_{3-\delta}$ sensor exhibited the best performance. The improved response was attributed to an increase in oxygen vacancies and the higher valence states of B-site cations induced by the A-site deficiency.[128]

Another perovskite material has also been studied for its $CO_2$ sensing ability. $BaTiO_3$ nanospheres, synthesized by a coprecipitate technique, showed high sensitivity and selectivity toward $CO_2$.[129] A heterostructure microsensor of CaO-$BaTiO_3$ showed high sensitivity and excellent selectivity toward $CO_2$ gas at 160 °C. The exceptional sensing performance was attributed to the precisely engineered *n-n* nanointerfaces and the optimized energy band alignment, which facilitate efficient charge transfer when exposed to $CO_2$ gas molecules, even at low concentrations.[130] Recently, pristine and Co-doped $PrFeO_3$ nanomaterials were synthesized via a sol−gel autocombustion route and were explored for the $CO_2$ gas sensor working at room temperature. The study indicated that the Co-doped sensor has a higher response and shorter recovery and response times.[131] The results obtained for $CO_2$ sensing properties of the perovskite materials have been summarized in Table 3.

**6.3. $NO_2$ Sensing Properties.** An investigation into the $NO_2$ sensing ability of perovskite-type $LnFeO_3$ (Ln = La, Nd, Sm, Gd, and Dy) powders revealed that the $SmFeO_3$ sensor exhibited the highest sensitivity.[132] Porous hollow microspheres of $SmFeO_3$ were synthesized using a metal−organic framework (MOF) compound as a templating precursor. Gas sensors utilizing these microspheres demonstrated exceptional chemoresistive performance for $NO_2$ detection at 200 °C. The achieved performance included high sensitivity, with a response of 10.2 at 200 ppb and a detection limit as low as 50 ppb, along with excellent selectivity and relatively fast response and recovery times of 369 and 478 s, respectively.[133]

A GO/$SrTiO_3$ sensing device was created by using a simple and cost-effective method. The results revealed that pristine GO sensors exhibited weaker sensing capabilities compared to those decorated with $SrTiO_3$. Notably, the GO/$SrTiO_3$ sensor showed the highest response and sensitivity to $NO_2$. This improvement is attributed to the $SrTiO_3$ nanoparticles, which enhance the adsorption of nitrogen dioxide and facilitate charge transfer between the GO, $SrTiO_3$, and adsorbed $NO_2$ molecules. Additionally, the GO/$SrTiO_3$ sensors demonstrated a low detection limit of 72 ppb for $NO_2$ and maintained stable responses even under varying humidity levels.[134]

The investigation of the gas sensing performance of the screen-printed thick film of Sr-doped in $BaTiO_3$ nanostructures synthesized using a hydrothermal method at low temperature showed strong response toward $NO_2$ at room temperature at 0.2 M% of Sr doping. Strontium ($Sr^{2+}$) ions with smaller ionic radius replace barium ($Ba^{2+}$) ions, causing significant tetragonal distortion and lattice strain. This structural change increases ionic displacement at the B site of the $ABO_3$ lattice, leading to higher polarization and dipole moments at room temperature in Sr-doped $BaTiO_3$ compared to pristine $BaTiO_3$, which shows a maximum dielectric constant only at ∼130 °C. Enhanced polarization at room temperature facilitates adsorption of $NO_2$ and $NH_3$ gases on the surface of Sr-doped $BaTiO_3$ nanomaterials. Conversely, as polarization diminishes at higher temperatures, gas adsorption decreases.[135]

$NO_2$ sensing properties of the $LaFeO_3$ synthesized on a silicon substrate using the radio frequency magnetron sputtering technique revealed that nanocubes of $LaFeO_3$ exhibited good performance toward 1 ppm of $NO_2$ gas at room temperature. This remarkable performance is attributed to their porous structure, morphology of the surface, high surface-active sites, and the high concentration of oxygen vacancies.[136] Dhariwal et al. developed a room-temperature $NO_2$ gas sensor using a cotton-modified $LaFeO_3$ (CLFO) composite combined with MXene. The CLFO/MXene sensor, synthesized via a hydrothermal method, exhibited p-type behavior and excellent recoverability, achieving a 14.2-fold higher response at 5 ppm of $NO_2$. It demonstrated a rapid response time of 2.7 s, a recovery time of 6.2 s, and strong stability. The enhanced sensitivity was attributed to surface gas interactions, adsorption energy, and charge transfer mechanisms (Figure 10-C).[137] The results obtained for $NO_2$ sensing properties of the perovskite materials have been summarized in Table 4.

## 7. CHALLENGES AND FUTURE TRENDS

Despite significant advancements in perovskite oxide-based gas sensors, several challenges persist, limiting their practical applications. One of the most important issues is the effect of environmental factors such as humidity and temperature variations on sensor performance. High relative humidity often increases cross-sensitivity and reduces selectivity,[138,139]



https://doi.org/10.1021/acsomega.4c11667
ACS Omega 2025, 10, 13780−13796

while temperature changes can destabilize oxygen vacancies and alter adsorption mechanisms, leading to unstable responses.[140] Additionally, the long-term stability of perovskite-based sensors remains a concern, as prolonged exposure to reactive gases or harsh conditions can degrade material properties, impacting performance and reliability. The scalability of synthesis techniques also presents challenges, particularly for complex morphologies or nanostructures that require precise control, making large-scale production expensive and time-consuming.

Addressing these limitations requires innovative approaches. For example, developing humidity-tolerant materials through surface functionalization or hydrophobic coatings could reduce the cross-sensitivity problem. Enhancing the thermal stability of perovskite structures via doping or composite formation may improve their stability at varying temperatures. Moreover, utilization of advanced fabrication techniques, such as additive manufacturing (3D printing) or roll-to-roll processing, could enable the scalable production of nanostructured perovskite sensors at reduced costs. Using machine learning and computational modeling to predict optimal material compositions and morphologies for specific gases can accelerate the discovery of high-performance sensors.

Future trends in this field are likely to focus on multifunctional sensors capable of detecting multiple gases simultaneously with high selectivity and sensitivity. Additionally, the use of perovskite sensors in Internet of Things (IoT) platforms for real-time environmental monitoring can be useful. These smart systems could provide continuous feedback on air quality with applications ranging from industrial emission monitoring to indoor air purification. By addressing current challenges and embracing these emerging trends, perovskite oxide-based sensors can result in highly efficient, scalable, and useful tools for environmental and industrial applications.

## 8. CONCLUSION

Perovskite oxide-based materials have emerged as efficient materials for gas sensing, offering customizable structural and functional properties. Recent advances, such as tailored doping, morphological engineering, and the creation of heterojunctions, have significantly enhanced their performance metrics. The ability to tune oxygen vacancies, modulate band structures, and integrate catalytic elements has enabled superior sensitivity and selectivity toward critical gases such as VOCs, $NO_2$, and $CO_2$. Despite these advances, challenges such as humidity interference, long-term stability, and cost-effective scalability exist and need further research. Future research should focus on optimizing synthesis techniques, exploring novel dopants, and using advanced computational methods to predict and enhance material behavior. By addressing these challenges, perovskite materials can fully realize their potential as efficient and scalable solutions for diverse gas-sensing applications.

## ■ ASSOCIATED CONTENT

### Data Availability Statement

No data was used for the research described in the article.

## ■ AUTHOR INFORMATION


### Corresponding Author

**Manoj Kumar Mishra** − *Salale University, Fitche 251, Ethiopia;* orcid.org/0000-0002-4832-5117; Email: mkmishra@slu.edu.et

### Authors

**Nafis Ahmad** − *Department of Physics, College of Science, King Khalid University, Abha 61413, Saudi Arabia*

**Prakash Kanjariya** − *Marwadi University Research Center, Department of Physics, Faculty of Science Marwadi University, Rajkot 360003 Gujarat, India*

**G. Padma Priya** − *Department of Chemistry and Biochemistry, School of Sciences, JAIN (Deemed to be University), Bangalore 560027 Karnataka, India*

**Anjan Kumar** − *Department of electronics and communication engineering, GLA University, Mathura 281406, India*

**Rishabh Thakur** − *Centre for Research Impact & Outcome, Chitkara University Institute of Engineering and Technology, Chitkara University, Rajpura 140401 Punjab, India*

**RSK Sharma** − *Department of Chemistry, Raghu Engineering College, Visakhapatnam, Andhra Pradesh 531162, India*

**Mukesh Kumari** − *Department of Applied Sciences-Chemistry, NIMS Institute of Engineering & Technology, NIMS University Rajasthan, Jaipur 303121, India*

**Sharnjeet Kaur** − *Department of Applied Sciences, Chandigarh Engineering College, Chandigarh Group of Colleges-Jhanjeri, Mohali 140307 Punjab, India*

Complete contact information is available at: https://pubs.acs.org/10.1021/acsomega.4c11667


### Author Contributions

**Nafis Ahmad:** Conceptualization, Formal analysis, Validation, Writing − original draft; **Prakash Kanjariya:** Software, Methodology, Writing − original draft; **G. Padma Priya:** Visualization, Writing − original draft; **Anjan Kumar:** Validation, Writing − original draft; **Rishabh Thakur:** Writing − original draft, Visualization; **RSK Sharma:** Writing − original draft; **Mukesh Kumari:** Review and editing; **Sharnjeet Kaur:** Review and editing; **Manoj Kumar Mishra:** Supervision, Review and editing.

### Notes

The authors declare no competing financial interest.

## ■ ACKNOWLEDGMENTS

The authors extend their appreciation to the Deanship of Scientific Research and Graduate Studies at King Khalid University for funding this work through the Large Research group Project under grant number RGP. 2/315/45.

## ■ REFERENCES


(1) Liu, Y.; Ji, H.; Yuan, Z.; Meng, F. Conductometric butanone gas sensor based on $Co_3O_4$ modified $SnO_2$ hollow spheres with ppb-level detection limit. *Sens. Actuators, B* **2023**, *374*, 132787.

(2) An, D.; Liu, N.; Zhang, H.; Sun, Q.; Li, C.; et al. Enhanced n-butanol sensing performance of $SnO_2$-based gas sensors by doping $In_2O_3$ via co-precipitation method. *Sens. Actuators, B* **2021**, *340*, 129944.

(3) Souri, M.; Yamini, Y.; Amoli, H. S. The synergistic effect of Ce dopant/Cotton bio-template on the performance of the $SnO_2$ gas sensor for the detection of Ethanol. *Materials Science and Engineering: B* **2023**, *294*, 116501.

(4) Franco, M. A.; Conti, P. P.; Andre, R. S.; Correa, D. S. A review on chemiresistive ZnO gas sensors. *Sensors and Actuators Reports* **2022**, *4*, 100100.

(5) Hu, J.-Y.; Lei, H.; Zhang, H.-Y.; Xue, X.-X.; Wang, X.-P.; et al. High reliable gas sensor based on crystal-facet regulated $\alpha$-$Fe_2O_3$ nanocrystals for rapid detection of exhaled acetone. *Rare Metals* **2024**, *43*, 6500−6515.

(6) Kong, L.; Yuan, Z.; Gao, H.; Meng, F. Recent progress of gas sensors based on metal oxide composites derived from bimetallic metal-organic frameworks. *TrAC Trends in Analytical Chemistry* **2023**, *166*, 117199.
(7) Cruz-Martínez, H.; Rojas-Chávez, H.; Montejo-Alvaro, F.; Peña-Castañeda, Y. A.; Matadamas-Ortiz, P. T.; Medina, D. I. Recent developments in graphene-based toxic gas sensors: a theoretical overview. *Sensors* **2021**, *21* (6), 1992.
(8) Siddique, I. Carbon nanotube-based sensors-A review. *Chemistry Research Journal* **2021**, *6* (1), 197−205.
(9) Souri, M.; Salar Amoli, H.; Yamini, Y. Three-dimensionally ordered porous In-doped $SmFeO_3$ perovskite gas sensor for highly sensitive and selective detection of formaldehyde. *Sens. Actuators, B* **2024**, *404*, 135213.
(10) Shinde, P. V.; Patra, A.; Rout, C. S. A review on the sensing mechanisms and recent developments on metal halide-based perovskite gas sensors. *Journal of Materials Chemistry C* **2022**, *10* (28), 10196−10223.
(11) Yadav, P.; Yadav, S.; Atri, S.; Tomar, R. A brief review on key role of perovskite oxides as catalyst. *ChemistrySelect* **2021**, *6* (45), 12947−12959.
(12) Chen, T.-W.; Ramachandran, R.; Chen, S.-M.; Anushya, G.; Ramachandran, K. Graphene and perovskite-based nanocomposite for both electrochemical and gas sensor applications: An overview. *Sensors* **2020**, *20* (23), 6755.
(13) Duan, X.; Jiang, Y.; Liu, B.; Duan, Z.; Zhang, Y.; et al. Enhancing the carbon dioxide sensing performance of $LaFeO_3$ by Co doping. *Sens. Actuators, B* **2024**, *402*, 135136.
(14) Gildo-Ortiz, L.; Ramírez-Ortega, J. A.; Guillén Bonilla, H.; Rodríguez-Betancourtt, V. M. Gas response enhancement of nano-crystalline $LaFeO_3$ perovskite prepared using the microwave-assisted solution method. *J Mater Sci: Mater Electron* **2023**, *34* (11), 959.
(15) Rong, Q.; Zhang, Y.; Hu, J.; Wang, H.; Zhu, Z.; et al. A double perovskite $LaFe_{1-x}SnxO_3$ nanocomposite modified by Ag for fast and accurate methanol detection. *Mater. Res. Bull.* **2020**, *132*, 111006.
(16) Argyrou, A.; Brintakis, K.; Kostopoulou, A.; Gagaoudakis, E.; Demeridou, I.; et al. Highly sensitive ozone and hydrogen sensors based on perovskite microcrystals directly grown on electrodes. *Journal of Materiomics* **2022**, *8* (2), 446−453.
(17) Porta, P.; Cimino, S.; De Rossi, S.; Faticanti, M.; Minelli, G.; Pettiti, I. $AFeO_3$ (A= La, Nd, Sm) and $LaFe_{1-x}MgxO_3$ perovskites: structural and redox properties. *Materials chemistry and physics* **2001**, *71* (2), 165−173.
(18) Natile, M. M.; Ponzoni, A.; Concina, I.; Glisenti, A. Chemical Tuning versus Microstructure Features in Solid-State Gas Sensors: $LaFe_{1-x}Ga_xO_3$, a Case Study. *Chem. Mater.* **2014**, *26* (4), 1505−1513.
(19) Ji, Q.; Bi, L.; Zhang, J.; Cao, H.; Zhao, X. S. The role of oxygen vacancies of $ABO_3$ perovskite oxides in the oxygen reduction reaction. *Energy Environ. Sci.* **2020**, *13* (5), 1408−1428.
(20) Hwang, J.; Feng, Z.; Charles, N.; Wang, X. R.; Lee, D.; et al. Tuning perovskite oxides by strain: Electronic structure, properties, and functions in (electro) catalysis and ferroelectricity. *Mater. Today* **2019**, *31*, 100−118.
(21) Kim, H. J.; Kim, U.; Kim, T. H.; Kim, J.; Kim, H. M.; et al. Physical properties of transparent perovskite oxides (Ba, La) $SnO_3$ with high electrical mobility at room temperature. *Phys. Rev. B* **2012**, *86* (16), 165205.
(22) Kuklja, M. M.; Mastrikov, Y. A.; Jansang, B.; Kotomin, E. A. The Intrinsic Defects, Disordering, and Structural Stability of $Ba_xSr_{1-x}Co_yFe_{1-y}O_{3-\delta}$ Perovskite Solid Solutions. *J. Phys. Chem. C* **2012**, *116* (35), 18605−18611.
(23) Hashtroudi, H.; Mackinnon, I. D.; Shafiei, M. Emerging 2D hybrid nanomaterials: towards enhanced sensitive and selective conductometric gas sensors at room temperature. *Journal of Materials Chemistry C* **2020**, *8* (38), 13108−13126.
(24) Zhu, J.; Li, H.; Zhong, L.; Xiao, P.; Xu, X.; et al. Perovskite oxides: preparation, characterizations, and applications in heterogeneous catalysis. *ACS Catal.* **2014**, *4* (9), 2917−2940.
(25) Hübner, M.; Simion, C. E.; Tomescu-Stănoiu, A.; Pokhrel, S.; Bârsan, N.; Weimar, U. Influence of humidity on CO sensing with p-type CuO thick film gas sensors. *Sens. Actuators, B* **2011**, *153* (2), 347−353.
(26) Wawrzyniak, J. Advancements in improving selectivity of metal oxide semiconductor gas sensors opening new perspectives for their application in food industry. *Sensors* **2023**, *23* (23), 9548.
(27) Singh, P.; Bansal, N. K.; Dey, S.; Singh, R.; Singh, T. Recent Progress on Perovskite Materials for VOC Gas Sensing. *Langmuir* **2024**, *40* (42), 21931−21956.
(28) Souri, M.; Salar Amoli, H. Gas sensing mechanisms in $ABO_3$ perovskite materials at room temperature: A review. *Materials Science in Semiconductor Processing* **2023**, *156*, 107271.
(29) Sato, T.; Takagi, S.; Deledda, S.; Hauback, B. C.; Orimo, S.-i. Extending the applicability of the Goldschmidt tolerance factor to arbitrary ionic compounds. *Sci. Rep.* **2016**, *6* (1), 23592.
(30) Hanmandlu, C.; Singh, A.; Boopathi, K. M.; Lai, C.-S.; Chu, C.-W. Layered perovskite materials: key solutions for highly efficient and stable perovskite solar cells. *Rep. Prog. Phys.* **2020**, *83* (8), 086502.
(31) Vasala, S.; Karppinen, M. $A_2B'B''O_6$ perovskites: a review. *Progress in solid state chemistry* **2015**, *43* (1−2), 1−36.
(32) Sengodan, S.; Choi, S.; Jun, A.; Shin, T. H.; Ju, Y.-W.; et al. Layered oxygen-deficient double perovskite as an efficient and stable anode for direct hydrocarbon solid oxide fuel cells. *Nature materials* **2015**, *14* (2), 205−209.
(33) Sharma, M.; Pathak, M.; Kapoor, P. N. The sol-gel method: pathway to ultrapure and homogeneous mixed metal oxide nano-particles. *Asian J. Chem.* **2018**, *30* (7), 1405−1412.
(34) Varma, A.; Mukasyan, A. S.; Rogachev, A. S.; Manukyan, K. V. Solution combustion synthesis of nanoscale materials. *Chem. Rev.* **2016**, *116* (23), 14493−14586.
(35) Eerenstein, W.; Mathur, N.; Scott, J. F. Multiferroic and magnetoelectric materials. *nature* **2006**, *442* (7104), 759−765.
(36) Chung, N. T. K.; Trinh, T. D.; Mittova, V. O.; Tomina, E. V.; Mittova, I. Y.; et al. Physicochemical characteristics of $DyFeO_3$ perovskite nanoparticles synthesized by a simple co-precipitation method at room temperature. *Emergent Materials* **2024**, *7*, 2767.
(37) Guo, J.; Ma, S.; Ma, N.; Liu, J.; Wei, J.; et al. Hydrothermal synthesis of NdFeO3 nanoparticles and their high gas-sensitive properties. *Ceram. Int.* **2024**, *50* (21), 43654−43664.
(38) Prince, A. G.; Durai, L.; Badhulika, S. Solid state synthesis of a $RuNiO_3$ perovskite nanomaterial as an electro-catalyst for direct alcohol (ethanol, methanol and ethylene glycol) fuel cell applications. *New J. Chem.* **2023**, *47* (8), 3870−3879.
(39) Domínguez-Crespo, M. A.; Torres-Huerta, A. M.; Brachetti-Sibaja, S. B.; Rodríguez-Salazar, A. E.; Gutiérrez-Galicia, F.; et al. Developing $ABO_3$ perovskites synthesized by the Pechini method for their potential application as cathode material in solid oxide fuel cells: Structural and electrical properties. *Boletín de la Sociedad Española de Cerámica y Vidrio* **2024**, *63* (2), 145−158.
(40) Chaudhari, G.; Jagtap, S.; Gedam, N.; Pawar, M.; Sangawar, V. Sol−gel synthesized semiconducting $LaCo_{0.8}Fe_{0.2}O_3$-based powder for thick film $NH_3$ gas sensor. *Talanta* **2009**, *78* (3), 1136−1140.
(41) Lippert, T.; Montenegro, M.; Döbeli, M.; Weidenkaff, A.; Müller, S.; et al. Perovskite thin films deposited by pulsed laser ablation as model systems for electrochemical applications. *Progress in solid state chemistry* **2007**, *35* (2−4), 221−231.
(42) Nieto, S.; Polanco, R.; Roque-Malherbe, R. Absorption kinetics of hydrogen in nanocrystals of $BaCe_{0.95}Yb_{0.05}O_{3-\delta}$ proton-conducting perovskite. *J. Phys. Chem. C* **2007**, *111* (6), 2809−2818.
(43) Kamble, V.; Zemase, R.; Gupta, R.; Aghav, B.; Shaikh, S.; et al. Improved toxic $NO_2$ gas sensing response of Cu-doped ZnO thin-film sensors derived by simple co-precipitation route. *Opt. Mater.* **2022**, *131*, 112706.
(44) Pérez-Coll, D.; Núñez, P.; Frade, J.; Abrantes, J. Conductivity of CGO and CSO ceramics obtained from freeze-dried precursors. *Electrochim. Acta* **2003**, *48* (11), 1551−1557.
(45) Haron, W.; Wisitsoraat, A.; Wongnawa, S. Nanostructured perovskite oxides−$LaMO_3$ (M= Al, Co, Fe) prepared by co-


https://doi.org/10.1021/acsomega.4c11667
*ACS Omega* 2025, 10, 13780−13796

precipitation method and their ethanol-sensing characteristics. *Ceram. Int.* **2017**, *43* (6), 5032−5040.
(46) Shi, C.; Hou, X.; Guo, R.; Zhang, W.; Zhou, Y. Starfish-like Zn doped $In_2O_3$ dendritic structure for superior triethylamine sensing by the facile co-precipitation method. *Mater. Res. Bull.* **2024**, *173*, 112668.
(47) Shandilya, M.; Rai, R.; Singh, J. Hydrothermal technology for smart materials. *Advances in Applied Ceramics* **2016**, *115* (6), 354−376.
(48) Guan, H.; Zhao, S.; Wang, H.; Yan, D.; Wang, M.; Zang, Z. Room temperature synthesis of stable single silica-coated $CsPbBr_3$ quantum dots combining tunable red emission of Ag−In−Zn−S for High-CRI white light-emitting diodes. *Nano Energy* **2020**, *67*, 104279.
(49) Danks, A. E.; Hall, S. R.; Schnepp, Z. The evolution of 'sol−gel'chemistry as a technique for materials synthesis. *Materials Horizons* **2016**, *3* (2), 91−112.
(50) Esposito, S. "Traditional" sol-gel chemistry as a powerful tool for the preparation of supported metal and metal oxide catalysts. *Materials* **2019**, *12* (4), 668.
(51) Patil, S. S.; Babar, B. M.; Nadargi, D. Y.; Shaikh, F. I.; Nadargi, J. D.; et al. La-Fe-O Perovskite Based Gas Sensors: Recent Advances and Future Challenges. *ACS omega* **2024**, *9* (28), 29994−30014.
(52) Ertl, G., Knözinger, H., Schüth, F.; et al., Eds. *Handbook of heterogeneous catalysis*; Wiley, 2008. DOI: 10.1002/9783527610044
(53) More, M. A.; More, S. A.; Femi, M. D.; Jain, G. H.; Aher, Y. B.; et al. Influence of the variation in hydrothermal reaction time on the structural, optical and electrical properties of $NiTiO_3$ perovskite and its application for gas sensing. *Interactions* **2024**, *245* (1), 358.
(54) Koyanagi, G. K.; Bohme, D. K. Gas-phase reactions of carbon dioxide with atomic transition-metal and main-group cations: room-temperature kinetics and periodicities in reactivity. *J. Phys. Chem. A* **2006**, *110* (4), 1232−1241.
(55) Kemnitz, E.; Noack, J. The non-aqueous fluorolytic sol−gel synthesis of nanoscaled metal fluorides. *Dalton Transactions* **2015**, *44* (45), 19411−19431.
(56) Bokov, D.; Turki Jalil, A.; Chupradit, S.; Suksatan, W.; Javed Ansari, M.; et al. Nanomaterial by sol-gel method: synthesis and application. *Advances in materials science and engineering* **2021**, *2021* (1), 5102014.
(57) Sunde, T. O. L.; Grande, T.; Einarsrud, M.-A. Modified Pechini synthesis of oxide powders and thin films. *Handbook of sol-gel science and technology*; Klein, L., Aparicio, M., Jitianu, A., Eds.; Springer, 2016. DOI: 10.1007/978-3-319-19454-7_130-1
(58) Qian, Y.; Ruan, Q.; Xue, M.; Chen, L. Emerging perovskite materials for supercapacitors: Structure, synthesis, modification, advanced characterization, theoretical calculation and electrochemical performance. *Journal of Energy Chemistry* **2024**, *89*, 41−70.
(59) Feinle, A.; Elsaesser, M. S.; Huesing, N. Sol−gel synthesis of monolithic materials with hierarchical porosity. *Chem. Soc. Rev.* **2016**, *45* (12), 3377−3399.
(60) Koli, P. B.; Kapadnis, K. H.; Deshpande, U. G.; Tupe, U. J.; Shinde, S. G.; Ingale, R. S. Fabrication of thin film sensors by spin coating using sol-gel $LaCrO_3$ Perovskite material modified with transition metals for sensing environmental pollutants, greenhouse gases and relative humidity. *Environmental Challenges* **2021**, *3*, 100043.
(61) Yadav, A. K.; Kumar, U.; Yadav, B. Sol−gel-processed CNT-doped $LaFeO_3$ and its application as LPG sensor. *Journal of Materials Science: Materials in Electronics* **2025**, *36* (1), 54.
(62) Alammar, T.; Hamm, I.; Grasmik, V.; Wark, M.; Mudring, A.-V. Microwave-assisted synthesis of perovskite $SrSnO_3$ nanocrystals in ionic liquids for photocatalytic applications. *Inorg. Chem.* **2017**, *56* (12), 6920−6932.
(63) Schmidt, R.; Prado-Gonjal, J.; Morán, E. Microwave assisted hydrothermal synthesis of nanoparticles. *arXiv*, 2022. DOI: 10.48550/arXiv.2203.02394
(64) Huang, X.; Zhao, G.; Wang, G.; Irvine, J. T. Synthesis and applications of nanoporous perovskite metal oxides. *Chemical science* **2018**, *9* (15), 3623−3637.
(65) Navas, D.; Fuentes, S.; Castro-Alvarez, A.; Chavez-Angel, E. Review on sol-gel synthesis of perovskite and oxide nanomaterials. *Gels* **2021**, *7* (4), 275.
(66) Abbas, H.; Youssef, A.; Hammad, F.; Hassan, A.; Hanafi, Z. Electrical properties of nano-sized indium tin oxide (ITO) doped with CuO, $Cr_2O_3$ and $ZrO_2$. *J. Nanopart. Res.* **2014**, *16*, 1−11.
(67) Derakhshi, Z.; Baghshahi, S.; Khodadadi, A. A.; Tamizifar, M. Cu-doped $LaFe_{1-x}Cu_xO_3$ perovskites nano-crystallites for enhanced VOCs detection. *Ceram. Int.* **2024**, *50* (13), 23175−23187.
(68) Bhardwaj, N.; Kundu, S. C. Electrospinning: A fascinating fiber fabrication technique. *Biotechnology advances* **2010**, *28* (3), 325−347.
(69) Han, T.; Ma, S.; Xu, X.; Cao, P.; Liu, W.; et al. Electrospinning synthesis, crystal structure, and ethylene glycol sensing properties of orthorhombic $SmBO_3$ (BFe, Co) perovskites. *J. Alloys Compd.* **2021**, *876*, 160211.
(70) Therese, G. H. A.; Dinamani, M.; Vishnu Kamath, P. Electrochemical synthesis of perovskite oxides. *Journal of applied electrochemistry* **2005**, *35*, 459−465.
(71) Gong, C.; Zhang, Z.; Lin, S.; Wu, Z.; Sun, L.; et al. Electrochemical synthesis of perovskite $LaFeO_3$ nanoparticle-modified $TiO_2$ nanotube arrays for enhanced visible-light photocatalytic activity. *New J. Chem.* **2019**, *43* (42), 16506−16514.
(72) Kalinina, E.; Pikalova, E. Opportunities, challenges and prospects for electrodeposition of thin-film functional layers in solid oxide fuel cell technology. *Materials* **2021**, *14* (19), 5584.
(73) Sasaki, T.; Matsumoto, Y.; Hombo, J.; Ogawa, Y. A new preparation method of LaMnO3 perovskite using electrochemical oxidation. *Journal of solid state chemistry* **1991**, *91* (1), 61−70.
(74) SASAKI, T.; MORIKAWA, T.; HOMBO, J.; MATSUMOTO, Y. Electrochemical Synthesis of $La_{1-x}Sr_xMnO_3$ Perovskite Films. *Denki Kagaku oyobi Kogyo Butsuri Kagaku* **1990**, *58* (6), 567−568.
(75) Matsumoto, Y.; Sasaki, T.; Hombo, J. A new preparation method of lanthanum cobalt oxide, $LaCoO_3$, perovskite using electrochemical oxidation. *Inorg. Chem.* **1992**, *31* (5), 738−741.
(76) Yang, K.; Ma, J.; Qiao, X.; Cui, Y.; Jia, L.; Wang, H. Hierarchical porous $LaFeO_3$ nanostructure for efficient trace detection of formaldehyde. *Sens. Actuators, B* **2020**, *313*, 128022.
(77) Guan, W.; Tang, N.; He, K.; Hu, X.; Li, M.; Li, K. Gas-sensing performances of metal oxide nanostructures for detecting dissolved gases: a mini review. *Frontiers in chemistry* **2020**, *8*, 76.
(78) Saruhan, B.; Lontio Fomekong, R.; Nahirniak, S. Influences of semiconductor metal oxide properties on gas sensing characteristics. *Frontiers in Sensors* **2021**, *2*, 657931.
(79) Degler, D.; Weimar, U.; Barsan, N. Current understanding of the fundamental mechanisms of doped and loaded semiconducting metal-oxide-based gas sensing materials. *ACS sensors* **2019**, *4* (9), 2228−2249.
(80) Liu, H.; Cao, Y.; Chen, Y.; Liu, W.; Miao, T.; et al. Gas response of $La_{1-x}Y_xFeO_3$ planar electrode sensors to volatile organic compounds under light illumination. *J. Alloys Compd.* **2023**, *937*, 168436.
(81) Qin, W.; Yuan, Z.; Shen, Y.; Zhang, R.; Meng, F. Phosphorus-doped porous perovskite $LaFe_{1-x}P_xO_{3-\delta}$ nanosheets with rich surface oxygen vacancies for ppb level acetone sensing at low temperature. *Chemical Engineering Journal* **2022**, *431*, 134280.
(82) Sun, L.; Qin, H.; Wang, K.; Zhao, M.; Hu, J. Structure and electrical properties of nanocrystalline $La_{1-x}Ba_xFeO_3$ for gas sensing application. *Mater. Chem. Phys.* **2011**, *125* (1−2), 305−308.
(83) Tang, W.; Liu, H.; Li, C.; Zhang, Y.; Sun, H.; et al. Facile synthesis of $LaNi_{1-x}Ti_xO_3$ nanoparticles and enhanced ethanol-sensing characteristics. *J. Phys. Chem. Solids* **2019**, *134*, 5−13.
(84) Xiaofeng, W.; MA, W.; SUN, K.; HU, J.; QIN, H. Nanocrystalline $Gd_{1-x}Ca_xFeO_3$ sensors for detection of methanol gas. *Journal of Rare Earths* **2017**, *35* (7), 690−696.
(85) Dey, S.; Roy, S. C. Influence of Ce doping on morphology, crystallinity and photoelectrochemical charge transfer characteristics of $TiO_2$ nanorod arrays grown on conductive glass substrate. *J. Alloys Compd.* **2021**, *881*, 160481.
(86) Porwal, S.; Bansal, N. K.; Ghosh, S.; Singh, T. Stress-induced stabilization of the photoactive $FAPbI_3$ phase under ambient conditions without using an additive approach. *Energy Advances* **2024**, *3* (4), 894−903.

(87) Bansal, N. K.; Porwal, S.; Singh, T. N-Methyl-2-pyrrolidone driven solvent engineering of hybrid perovskite solar cells fabricated under air ambient conditions. *Surfaces and Interfaces* **2024**, *44*, 103738.
(88) Noh, K. W., Defect engineering of metal oxide semiconductors, M.S. Thesis, University of Illinois at Urbana-Champaign, 2010.
(89) Dey, S.; Chakravorty, A.; Mishra, S. B.; Khatun, N.; Hazra, A.; et al. Localized thermal spike driven morphology and electronic structure transformation in swift heavy ion irradiated $TiO_2$ nanorods. *Nanoscale Advances* **2021**, *4* (1), 241−249.
(90) Yamazoe, N.; Shimanoe, K. Theory of power laws for semiconductor gas sensors. *Sens. Actuators, B* **2008**, *128* (2), 566−573.
(91) Tang, F.; Cai, Y.; Tang, X.; Zhang, M. Rich surface oxygen vacancies $SmFeO_3$ for acetylene gas sensor with ppb-level detection. *Sens. Actuators, B* **2025**, *422*, 136708.
(92) Xuan, W.; Shan, H.; Hu, D.; Zhu, L.; Guan, T.; et al. In-situ synthesis of stable ZnO-coated $CsPbBr_3$ nanocrystals for room-temperature heptanal sensors. *Materials Today Chemistry* **2022**, *26*, 101155.
(93) Ji, H.; Zhang, L.; Zhang, R. Gas sensitive performance and mechanism of multiferroic $BiFeO_3$ under thermal-magnetic synergetic excitation. *Inorg. Chem. Commun.* **2023**, *150*, 110491.
(94) Lin, T.; Lv, X.; Li, S.; Wang, Q. The morphologies of the semiconductor oxides and their gas-sensing properties. *Sensors* **2017**, *17* (12), 2779.
(95) Chen, Y.; Xia, H.; Lu, L.; Xue, J. Synthesis of porous hollow $Fe_3O_4$ beads and their applications in lithium ion batteries. *J. Mater. Chem.* **2012**, *22* (11), 5006−5012.
(96) Zou, F.; Chen, Y.-M.; Liu, K.; Yu, Z.; Liang, W.; et al. Metal organic frameworks derived hierarchical hollow NiO/Ni/graphene composites for lithium and sodium storage. *ACS Nano* **2016**, *10* (1), 377−386.
(97) Han, L.; Yu, X.-Y.; Lou, X. W. Formation of Prussian-Blue-Analog Nanocages via a Direct Etching Method and their Conversion into Ni-Co-Mixed Oxide for Enhanced Oxygen Evolution. *Advanced Materials (Deerfield Beach, Fla.)* **2016**, *28* (23), 4601−4605.
(98) Lee, J.; Farha, O. K.; Roberts, J.; Scheidt, K. A.; Nguyen, S. T.; Hupp, J. T. Metal−organic framework materials as catalysts. *Chem. Soc. Rev.* **2009**, *38* (5), 1450−1459.
(99) Furukawa, H.; Cordova, K. E.; O'Keeffe, M.; Yaghi, O. M. The chemistry and applications of metal-organic frameworks. *Science* **2013**, *341* (6149), 1230444.
(100) Kreno, L. E.; Leong, K.; Farha, O. K.; Allendorf, M.; Van Duyne, R. P.; Hupp, J. T. Metal−organic framework materials as chemical sensors. *Chem. Rev.* **2012**, *112* (2), 1105−1125.
(101) Kim, M.; Park, S.; Ahn, J.; Baek, J. W.; Kim, D.-H.; et al. Vitalizing Perovskite Oxide-Based Acetone Sensors with Metal−Organic Framework-Derived Heterogeneous Oxide Catalysts. *ACS Sensors* **2024**, *9* (12), 6492−6501.
(102) Guo, R.; Wang, H.; Tian, R.; Shi, D.; Li, H.; et al. The enhanced ethanol sensing properties of CNT@ $ZnSnO_3$ hollow boxes derived from Zn-MOF (ZIF-8). *Ceram. Int.* **2020**, *46* (6), 7065−7073.
(103) Fan, H.-T.; Xu, X.-J.; Ma, X.-K.; Zhang, T. Preparation of $LaFeO_3$ nanofibers by electrospinning for gas sensors with fast response and recovery. *Nanotechnology* **2011**, *22* (11), 115502.
(104) Cao, E.; Chu, Z.; Wang, H.; Hao, W.; Sun, L.; Zhang, Y. Effect of film thickness on the electrical and ethanol sensing characteristics of $LaFeO_3$ nanoparticle-based thick film sensors. *Ceram. Int.* **2018**, *44* (6), 7180−7185.
(105) Phan, T. T. N.; Dinh, T. T. M.; Nguyen, M. D.; Li, D.; Phan, C. N.; et al. Hierarchically structured $LaFeO_3$ with hollow core and porous shell as efficient sensing material for ethanol detection. *Sens. Actuators, B* **2022**, *354*, 131195.
(106) Chen, M.; Wang, H.; Hu, J.; Zhang, Y.; Li, K.; et al. Near-room-temperature ethanol gas sensor based on mesoporous Ag/Zn−$LaFeO_3$ nanocomposite. *Advanced Materials Interfaces* **2019**, *6* (1), 1801453.
(107) Soni, V.; Singh, P.; Shree, V.; Goel, V. Effects of VOCs on human health. *Air pollution and control* **2018**, 119−142.
(108) Tsai, W.-T. An overview of health hazards of volatile organic compounds regulated as indoor air pollutants. *Reviews on environmental health* **2019**, *34* (1), 81−89.
(109) Adiguzel, Y.; Kulah, H. Breath sensors for lung cancer diagnosis. *Biosens. Bioelectron.* **2015**, *65*, 121−138.
(110) Chaudhary, V.; Taha, B. A.; Lucky; Rustagi, S.; Khosla, A.; et al. Nose-on-Chip Nanobiosensors for Early Detection of Lung Cancer Breath Biomarkers. *ACS sensors* **2024**, *9* (9), 4469−4494.
(111) Song, J.; Li, R.; Yu, R.; Zhu, Q.; Li, C.; et al. Detection of VOCs in exhaled breath for lung cancer diagnosis. *Microchemical Journal* **2024**, *199*, 110051.
(112) Singh, P.; Bansal, N. K.; Dey, S.; Singh, R.; Singh, T. Recent Progress on Perovskite Materials for VOC Gas Sensing. *Langmuir* **2024**, *40* (42), 21931−21956.
(113) Chen, L.; Hu, J.; Fang, S.; Han, Z.; Zhao, M.; et al. Ethanol-sensing properties of $SmFe_{1-x}Ni_xO_3$ perovskite oxides. *Sens. Actuators, B* **2009**, *139* (2), 407−410.
(114) Hao, P.; Qiu, G.; Song, P.; Yang, Z.; Wang, Q. Construction of porous $LaFeO_3$ microspheres decorated with NiO nanosheets for high response ethanol gas sensors. *Appl. Surf. Sci.* **2020**, *515*, 146025.
(115) Yuan, Z.; Chu, N.; Meng, F. Improvement in the performance of $In_2O_3$ ethanol sensor by perovskite-type $LaFeO_3$ modification and sensitivity mechanism analysis. *Sens. Actuators, B* **2024**, *406*, 135415.
(116) Li, K.; Wu, Y.; Chen, M.; Rong, Q.; Zhu, Z.; et al. High methanol gas-sensing performance of $Sm_2O_3$/ZnO/$SmFeO_3$ microspheres synthesized via a hydrothermal method. *Nanoscale Res. Lett.* **2019**, *14*, 1−13.
(117) Xiao, C.; Ma, Z.; Gao, X.; Zou, P.; Jia, L. Fabrication of Pt functionalized $LaFeO_3$ porous structures for highly sensitive detection of formaldehyde. *Sens. Actuators, B* **2024**, *410*, 135644.
(118) Dash, S.; Mojumder, S.; Das, T.; Saha, D.; Pal, M. Highly sensitive and selective rGO-$LaFeO_3$ nanocomposite based formaldehyde sensors towards air quality monitoring. *Chemosphere* **2024**, *367*, 143499.
(119) Xukeer, A.; Li, J. Rapid $YFeO_3$ gas sensor for detecting formaldehyde working at room temperature. *Curr. Appl. Phys.* **2024**, *63*, 116−125.
(120) Xiao, C.; Zhang, X.; Ma, Z.; Yang, K.; Gao, X.; et al. Formaldehyde gas sensor with 1 ppb detection limit based on In-doped $LaFeO_3$ porous structure. *Sens. Actuators, B* **2022**, *371*, 132558.
(121) Li, X.-B.; Zhou, H.; Huang, L.-L.; Gao, C.; Zhang, Q.-Q.; et al. Detection of formaldehyde sensitive properties of Sm3+ doped $NdFeO_3$. *J. Alloys Compd.* **2025**, *1010*, 176933.
(122) Wusiman, M.; Taghipour, F. Methods and mechanisms of gas sensor selectivity. *Critical Reviews in Solid State and Materials Sciences* **2022**, *47* (3), 416−435.
(123) Rong, Q.; Li, K.; Wang, C.; Zhang, Y.; Chen, M.; et al. Enhanced performance of an acetone gas sensor based on Ag-$LaFeO_3$ molecular imprinted polymers and carbon nanotubes composite. *Nanotechnology* **2020**, *31* (40), 405701.
(124) Meng, F.; Hu, J.; Liu, C.; Tan, Y.; Zhang, Y. Highly sensitive and low detection limit of acetone gas sensor based on porous $YbFeO_3$ nanocrystallines. *Chem. Phys. Lett.* **2021**, *780*, 138925.
(125) Cao, E.; Zhang, Y.; Zhang, Y.; Hao, W.; Sun, B.; Sun, L. Acetone sensing characteristics of $TiO_2$-$LaFeO_3$ nanocomposites. *Mater. Lett.* **2023**, *351*, 135056.
(126) Wu, H.; Meng, F.; Gong, X.; Tao, W.; Zhao, L.; et al. A solution to boost acetone sensing performance of perovskite oxides chemiresistors: In-situ derived pp heterostructures. *Sens. Actuators, B* **2023**, *378*, 133092.
(127) Wang, X.; Qin, H.; Sun, L.; Hu, J. $CO_2$ sensing properties and mechanism of nanocrystalline $LaFeO_3$ sensor. *Sens. Actuators, B* **2013**, *188*, 965−971.
(128) Jiao, A.; Zhang, Y.; Yang, L.; Zhao, X.; Wu, C.; et al. Enhanced CO2 response of $La_{1-x}FeO_{3-\delta}$ perovskites with A-site deficiency synthesized by flame spray pyrolysis. *Ceram. Int.* **2023**, *49* (1), 591−599.


https://doi.org/10.1021/acsomega.4c11667
*ACS Omega* 2025, 10, 13780−13796

(129) Rodrigues, J.; Shimpi, N. G. High Performance-Low Cost-Chemiresitive $BaTiO_3$ Nanospheres Based $CO_2$ Gas Sensor for Air Quality Monitoring. *ChemistrySelect* **2024**, *9* (40), No. e202401547.
(130) Joshi, S.; Antolasic, F.; Sunkara, M. V.; Bhargava, S. K.; Ippolito, S. J. Highly selective $CO_2$ gas sensing properties of CaO-$BaTiO_3$ heterostructures effectuated through discretely created nn nano-interfaces. *ACS Sustainable Chem. Eng.* **2018**, *6* (3), 4086−4097.
(131) Bharati, K.; Tiwari, P. R.; Singh, R. P.; Singh, A.; Yadav, B.; Kumar, S.; et al. Cobalt-doped praseodymium ortho ferrite as a promising nanomaterial for carbon dioxide gas sensing. *Journal of Materials Chemistry C* **2023**, *11* (44), 15581−15590.
(132) Aono, H.; Traversa, E.; Sakamoto, M.; Sadaoka, Y. Crystallographic characterization and NO2 gas sensing property of $LnFeO_3$ prepared by thermal decomposition of Ln— Fe hexacyanocomplexes, Ln [Fe (CN) 6]· $nH_2O$, Ln= La, Nd, Sm, Gd, and Dy. *Sens. Actuators, B* **2003**, *94* (2), 132−139.
(133) Huang, H.-T.; Zhang, W.-L.; Zhang, X.-D.; Guo, X. $NO_2$ sensing properties of SmFeO3 porous hollow microspheres. *Sens. Actuators, B* **2018**, *265*, 443−451.
(134) Kacem, K.; Casanova-Chafer, J.; Ameur, S.; Nsib, M. F.; Llobet, E. Gas sensing properties of graphene oxide loaded with $SrTiO_3$ nanoparticles. *J. Alloys Compd.* **2023**, *941*, 169011.
(135) Patil, R.; Gaikwad, S.; Karanjekar, A.; Khanna, P.; Jain, G.; et al. Optimization of strontium-doping concentration in $BaTiO_3$ nanostructures for room temperature $NH_3$ and $NO_2$ gas sensing. *Materials Today Chemistry* **2020**, *16*, 100240.
(136) Thirumalairajan, S.; Girija, K.; Mastelaro, V. R.; Ponpandian, N. Surface morphology-dependent room-temperature $LaFeO_3$ nanostructure thin films as selective $NO_2$ gas sensor prepared by radio frequency magnetron sputtering. *ACS Appl. Mater. Interfaces* **2014**, *6* (16), 13917−13927.
(137) Dhariwal, N.; Yadav, P.; Kumari, M.; Akanksha; Sanger, A.; et al. Engineering an Ultrafast Ambient $NO_2$ Gas Sensor Using Cotton-Modified $LaFeO_3$/MXene Composites. *ACS sensors* **2024**, *9* (12), 6800−6814.
(138) Duong, V. T.; Nguyen, C. T.; Luong, H. B.; Nguyen, D. C.; Nguyen, H. L. Ultralow-detection limit ammonia gas sensors at room temperature based on MWCNT/$WO_3$ nanocomposite and effect of humidity. *Solid State Sci.* **2021**, *113*, 106534.
(139) Boehme, I.; Weimar, U.; Barsan, N. Unraveling the surface chemistry of CO sensing with $In_2O_3$ based gas sensors. *Sens. Actuators, B* **2021**, *326*, 129004.
(140) Hossein-Babaei, F.; Ghafarinia, V. Compensation for the drift-like terms caused by environmental fluctuations in the responses of chemoresistive gas sensors. *Sens. Actuators, B* **2010**, *143* (2), 641−648.


https://doi.org/10.1021/acsomega.4c11667
*ACS Omega* 2025, 10, 13780−13796